Thesis for the Degree of Doctor of Philosophy

Correlative Chemical Imaging of Nanoscale Subcellular Structures

Stefania Rabasco

UNIVERSITY OF GOTHENBURG

Department of Chemistry and Molecular Biology

Gothenburg, 2023

Thesis for the Degree of Doctor of Philosophy

Correlative Chemical Imaging of Nanoscale Subcellular Structures

Stefania Rabasco

Cover illustration: Revisiting Plato's Allegory of the Cave in the realm of chemical imaging: exploring the “shadows” of cells (left). Examples of NanoSIMS images (right).

Stefania.rabasco@gu.se

ISBN 978-91-8069-299-1 (PRINT)
ISBN 978-91-8069-300-4 (PDF)
Available online at http://hdl.handle.net/2077/75348

Department of Chemistry and Molecular Biology
University of Gothenburg
SE-405 30 Göteborg, Sweden

Printed by Stema Specialtryck AB

“If I've learned one thing,
it's that before you get anywhere in life,
you got to stop listening to yourself.”

Jerry Smith

Abstract

Chemical imaging can elucidate complex mechanisms, relationships, and components of biological samples. For example, it can reveal properties such as chemical composition, chemical structure, reactivity, and topography. Several imaging techniques exist, each providing different types of information. Yet, no single technique can comprehensively characterize a sample. Having a holistic profile often requires correlating complementary methods; for example, scanning electron microscopy (SEM) can be combined with secondary ion mass spectrometry (SIMS) imaging to obtain insights on both the physical topography (*via* SEM) and the chemical composition (*via* SIMS) of a sample surface. This approach is referred to as correlative imaging.

Correlative chemical imaging is applicable in many scientific fields, such as biology, chemistry, geology, and material science. Among the wide variety of modern imaging techniques that exist, nanoscale SIMS (NanoSIMS) emerges as a powerful tool, having seen growing applications, especially in biochemistry and cell biology. To this end, it can be used for the detection of isotopically labeled material in a sample and provides the chemical composition of the sample surface with high lateral resolution (down to 50 nm), sensitivity (ppm-ppb range), and mass resolution (up to 10000). By using an isotopic label, target molecules in the sample can be studied, although unlabeled samples can be used in some cases. NanoSIMS presents some limitations; for example, it usually cannot discern the ultrastructure of very small, intricate sample details (*e.g.*, subcellular ultrastructure). Therefore, NanoSIMS is often correlated with additional imaging techniques, such as microscopy, to push its capabilities and overcome its shortcomings.

In the papers which are part of this thesis, NanoSIMS imaging was correlated with either electron or light microscopy to address different biological questions. To discern nanoscale subcellular ultrastructures, transmission electron microscopy (TEM) was employed, and to localize an organelle labeled with an antibody and a fluorescent tag, STED microscopy was used. In paper I, NanoSIMS was employed to detect ^{13}C-dopamine in PC12 cells, and the images correlated with TEM to

localize the dopamine within large dense core vesicles (LDCVs). In paper II, NanoSIMS was correlated with stimulated emission-depletion (STED) microscopy to localize endoplasmic reticulum stress-induced stress granules (SGs) in neuronal progenitor cells (NPCs) incubated with an isotopically labeled amino acid, and to characterize their protein turnover by changes in isotopic enrichment. In paper III, I investigated the role of vesicle size in the dynamics of partial release exocytosis events of PC12 cells by correlating TEM and NanoSIMS imaging data. In paper IV, NanoSIMS and TEM were correlated to look at the subcellular protein turnover in NPCs using different isotopically labeled amino acids and time-points. Overall, these studies demonstrate the importance of adequate correlative imaging strategies, and the variety of biological aims that can be achieved through different correlative chemical imaging approaches.

Sammanfattning på svenska

Kemisk avbildning kan belysa komplexa mekanismer, relationer och komponenter hos biologiska prover. Till exempel kan det avslöja provernasegenskaper såsom kemisk sammansättning, kemisk struktur, reaktivitet och form. Flera avbildningsmetoder finns tillgängliga, var och en som ger olika typer av information. Men ingen enskild teknik kan heltäckande karakterisera ett prov. Att ha en holistisk profil kräver ofta att man korrelerar kompletterande metoder; till exempel kan scanning electron microscopy (SEM) kombineras med bildbehandling med sekundärjoner (SIMS) för att erhålla insikter både om den fysiska formen (*via* SEM) och den kemiska sammansättningen (*via* SIMS) hos en provyta. Denna metod kallas korrelativ bildbehandling.

Korrelativ kemisk avbildning kan tillämpas inom många vetenskapliga områden, såsom biologi, kemi, geologi och materialvetenskap. Bland det stora utbudet av moderna avbildningsmetoder är nanoscale SIMS (NanoSIMS) ett kraftfullt verktyg som har sett ökande tillämpningar, särskilt inom biokemi och cellbiologi. För dessa ändamål kan det användas för detektion av isotopiskt märkt material i ett prov och ger den kemiska sammansättningen av provytan med hög lateral upplösning (ner till 50 nm), känslighet (ppm-ppb område) och massupplösning (upp till 10000). Genom att använda en isotopisk markör kan målmolekyler i provet studeras, även om omärkta prover kan användas i vissa fall. NanoSIMS har vissa begränsningar; till exempel kan den vanligtvis inte urskilja ultrastrukturen hos mycket små, intrikata provdetaljer (t.ex. subcellulär ultrastruktur). Därför korreleras NanoSIMS ofta med ytterligare bildbehandlingsmetoder, såsom mikroskopi, för att utöka dess kapacitet och övervinna dess brister.

I de artiklar som ingår i denna avhandling så korrelerades NanoSIMS-bildtagning med antingen elektronmikroskopi eller ljusmikroskopi för att besvara olika biologiska frågeställningar. För att skilja nanoskaliga subcellulära ultrastrukturer användes transmissions elektronmikroskopi (TEM), och för att lokalisera en organell märkt med ett antikropp och en fluorescerande markör användes STED-mikroskopi. I artikel I

användes NanoSIMS för att detektera ^{13}C-dopamin i PC12-celler, och bilderna korrelerades med TEM för att lokalisera dopaminet inom stora kompaktkärnade vesiklar (LDCVs). I artikel II korrelerades NanoSIMS med stimulated emission-depletion (STED) mikroskopi för att lokalisera stressgranula (SG) inducerade av endoplasmisk retikulum-stress i neuronal progenitorceller (NPCs) inkuberade med en isotopiskt märkt aminosyra och för att karakterisera deras proteinomsättning genom förändringar i isotopisk berikning. I artikel III undersöktes rollen av vesikelstorlek i dynamiken hos partiell frisättning i exocytosehändelser av PC12-celler genom att korrelera TEM- och NanoSIMS-bildtagning. I artikel IV korrelerades NanoSIMS och TEM för att undersöka den subcellulära proteinomsättningen i NPCs med hjälp av olika isotopiskt märkta aminosyror och tidpunkter. Sammanfattningsvis visar dessa studier vikten av adekvata korrelative avbildningsstrategier och den variation av biologiska mål som kan uppnås genom olika korrelera kemiska bildtagningstekniker.

List of Publications and Contribution Report

Published articles

I. Localization and Absolute Quantification of Dopamine in Discrete Intravesicular Compartments Using NanoSIMS Imaging
Stefania Rabasco, Tho D.K. Nguyen, Chaoyi Gu, Michael E. Kurczy, Nhu T.N. Phan and Andrew G. Ewing
International Journal of Molecular Sciences 2022, 23(1), p.160.

Participated in designing the TEM and NanoSIMS experiments, participated in performing the sample preparation, performed the TEM imaging, participated in performing the NanoSIMS imaging, performed the TEM/NanoSIMS data analysis, participated in the discussion of the results. Outlined and wrote the first draft of the manuscript. Edited the manuscript with the other authors.

II. Characterization of Stress Granule Protein Turnover in Neuronal Progenitor Cells Using Correlative STED and NanoSIMS Imaging
Stefania Rabasco, Alicia A. Lork, Emmanuel Berlin, Tho D.K. Nguyen, Nicolas Locker, Carl Ernst, Andrew G. Ewing and Nhu T.N. Phan
International Journal of Molecular Sciences 2023, 24(3), p.2546

Participated in designing the STED and NanoSIMS experiments, participated in performing the sample preparation, performed the NanoSIMS imaging, participated in the data analysis and the discussion of the results. Outlined and wrote the first draft of the manuscript. Edited the manuscript with the other authors.

Manuscripts submitted

III. Quantitative NanoSIMS Imaging of Individual Vesicles to Investigate the Relation between Fraction of Chemical Release and Vesicle Size
Tho D.K. Nguyen [¥], Stefania Rabasco [¥], Alicia A. Lork and Andrew G. Ewing

Participated in designing the TEM and NanoSIMS experiments, participated in performing the sample preparation and NanoSIMS imaging, performed the TEM imaging, participated in the data analysis and the discussion of the

results. Wrote the first draft of the manuscript with T.D.K.N. Edited the manuscript with the other authors.

Manuscripts in preparation

IV. Subcellular Spatial Distribution of Protein Turnover in Neuronal Progenitor Cells
Alicia A. Lork, Stefania Rabasco, Carl Ernst, Silvio O. Rizzoli and Nhu T.N. Phan

Participated in performing the sample preparation, performed the TEM imaging, participated in the discussion of the results. Edited the manuscript with the other authors.

[¥] *These authors contributed equally to the work*

Related Publications not included in the thesis

Chemical Analysis of Single Cells and Organelles
Keke Hu, Tho D.K. Nguyen, Stefania Rabasco, Pieter E. Oomen and Andrew G. Ewing
Analytical Chemistry 2020, *93*(1), pp.41-71.

Table of contents

ABBREVIATIONS ix

CHAPTER 1. Biological Chemical Imaging Techniques and Correlative Imaging 1

1.1 Overview 1

1.1.1 Types of Imaging Techniques and their Applications 1

1.1.2 Correlative Imaging 2

1.2 Mass Spectrometry Imaging (MSI) 3

1.2.1 Overview of SIMS history 3

1.2.2 Types of MSI: LDI, DESI, and SIMS 4

1.2.3 NanoSIMS 7

1.3 Microscopy 14

1.3.1 Overview 14

1.3.2 Types of Microscopy: EM, LM and SPM 15

1.3.3 Transmission Electron Microscopy (TEM) 17

1.3.4 Confocal and Stimulated Emission Depletion (STED) Microscopy 22

CHAPTER 2. Biological Systems Imaged in this Thesis 28

2.1 Overview 28

2.2 Immortal Cell Lines and Pheochromocytoma 12 (PC12) Cells 29

2.3 Stem Cells and Neuronal Progenitor Cells (NPCs) 32

CHAPTER 3. Sample Preparation 35

3.1 Principles of Biological Sample Preparation for Chemical Imaging 35

3.2 Cell Sample Preparation for Correlative TEM/FM and NanoSIMS 42

CHAPTER 4. Research Topics for the Application of Correlative NanoSIMS and EM/LM 46

4.1 Intercellular Communication 46

4.1.1 Vesicles, Neurotransmitters and Exocytosis 46

4.1.2 Application of Correlative Imaging for the Study of Cellular Communication 50

4.2 Cellular Stress, Stress Granules and Protein Turnover 53

4.2.1 Cellular Stress, RNP Granules and Mechanisms of Stress Granules 53

4.2.1 Application of Correlative Imaging for the Study of Cellular Stress 57

CHAPTER 5. Summary of Papers 59

5.1 Paper I 59

5.2 Paper II 59

5.3 Paper III 59

5.4 Paper IV 60

CHAPTER 6. Concluding Remarks and Future Outlook 61

Acknowledgments 62

References 64

ABBREVIATIONS

AFM – Atomic Force Microscopy

ALS – Amyotrophic Lateral Sclerosis

ATF6 – Activating Transcription Factor 6

ATP – Adenosine Triphosphate

CAPRIN – Cell Cycle Associated Protein

CgA – Chromogranin A

CLEM – Correlative Light and Electron Microscopy

CNS – Central Nervous System

CSR – Cellular Stress Response

DAPPI – Desorption Atmospheric Pressure Photoionization

DESI – Desorption Electrospray Ionization

EDXS – Energy Dispersive X-ray Spectroscopy

EM – Electron Microscopy

ER – Endoplasmic Reticulum

ESC – Embryonic Stem Cell

ESI – Electrospray Ionization

FISH – Fluorescence *In Situ* Hybridization

FM – Fluorescence Microscopy

FUS – Fused in Sarcoma

GA – Glutaraldehyde

G3BP1 – Ras GTPase-activating Protein-binding Protein 1

HEPES – 4-(2-hydroxyethyl)-1-piperazineethanesulfonic Acid

HPF – High Pressure Freezing

iPSC – Induced Pluripotent Stem Cell

IRE1 – Inositol-requiring Enzyme 1

LAESI – Laser Ablation Electrospray Ionization

LDI – Laser Desorption Ionization

L-DOPA – L-3,4-dihydroxyphenylalanine

LESA – Liquid Extraction Surface Analysis

LLPS – Liquid-liquid Phase Separation

LM – Light Microscopy

MALDI – Matrix Assisted Laser Desorption Ionization

MS – Mass Spectrometry

MSI – Mass Spectrometry Imaging

m/z – mass-to-charge

NA – Numerical Aperture

Nano-DESI – Nanospray Desorption Electrospray Ionization

NanoSIMS – Nanoscale Secondary Ion Mass Spectrometry

ND – Neurodegenerative Disease

NPC – Neuronal Progenitor Cell

PALM – Photoactivated Localization Microscopy

PBS – Phosphate-buffered Saline

PC12 – Pheochromocytoma 12

PERK – Protein Kinase RNA-like Endoplasmic Reticulum Kinase

PESI – Probe Electrospray Ionization

PFA – Paraformaldehyde

PIPES – 1,4-Piperazinediethanesulfonic Acid

QSA – Quasi Simultaneous Arrival

RBP – RNA-binding proteins

RNP – Ribonucleoprotein

ROI – Region of Interest

SEM – Scanning Electron Microscopy

SG – Stress Granule

SIMS – Secondary Ion Mass Spectrometry

SMAD – Small Worm Phenotype Mothers Against Decapentaplegic

SNARE – Soluble *N*-ethylmaleimide-sensitive Factor Attachment Protein Receptor

SPM – Scanning Probe Mircoscopy

STED – Stimulated Emission Depletion

STM – Scanning Tunneling Microscopy

STORM – Stochastic Optical Reconstruction Microscopy

TDP-43 – TAR DNA-binding Protein 43

TEM – Transmission Electron Microscopy

TIA-1 – T-cell Intracellular Antigen-1

ToF-SIMS – Time-of-Flight Secondary Ion Mass Spectrometry

UHV – ultrahigh vacuum

VAMP – Vesicle-associated Membrane Protein

Wnt – Wingless-related Integration Site

CHAPTER 1. Biological Chemical Imaging Techniques and Correlative Imaging

1.1 Overview

Analytical imaging is a term that encompasses a wide range of techniques used to analyze the properties of a sample. It is widely used in many scientific fields, such as biology, chemistry, geology, material science, environmental science, and medicine. The applications of imaging extend broadly. For example, it allows analyzing molecules in biological samples and localizing them in organs, tissues, or single cells, it can support the development of drugs and disease treatments, or characterize inorganic materials such as superconductors, minerals, and metals.[1–5] Therefore, imaging is a versatile tool that can be applied to a variety of aims and objectives. This thesis will discuss some chemical imaging techniques and describe how they were used correlatively to each other to answer different biochemical questions.

1.1.1 Types of Imaging Techniques and their Applications

Several modern analytical imaging techniques exist, each implemented in different ways. Categories of imaging include mass spectrometry imaging (MSI), microscopy, spectroscopy, and medical imaging. In MSI, typically an ion or laser beam interacts with a sample surface, causing molecules to sputter and be available for collection, detection, and analysis. Some examples include matrix assisted laser desorption ionization (MALDI) and time-of-flight secondary ion mass spectrometry (ToF-SIMS) imaging. MSI is further discussed in section *1.2 Mass Spectrometry Imaging (MSI)*. Microscopy includes techniques such as electron microscopy (EM) and light microscopy (LM). These are based on how a beam (an electron or light beam) interacts with a sample to produce an image. Different types of EM and LM have been developed; they are further described in section *1.3 Microscopy*. In spectroscopy, such as infrared and nuclear magnetic resonance spectroscopy, light is directed at a sample and the resulting interaction is used to identify the properties of atoms and molecules in the sample.

A variety of spectroscopy techniques exist, and these include infrared spectroscopy, Raman spectroscopy, and nuclear magnetic resonance spectroscopy. Medical imaging refers to a collection of techniques which are mostly used in diagnostics and clinical analysis. Functional medical imaging can detect changes in physiological activity (such as metabolism, hemodynamics and oxygen levels) in tissues and organs; some common functional imaging techniques are positron emission tomography and functional magnetic resonance imaging. Another type of medical imaging, called structural imaging, visualizes anatomical properties (such as structural damage or abnormalities) of tissues and organs; examples include computed tomography and structural magnetic resonance imaging.[6–8] Spectroscopy and medical imaging are beyond the scope of this thesis and thus will not be discussed further.

1.1.2 Correlative Imaging

While a great deal of information can be obtained with imaging, every technique has limitations. These can be related to aspects such as sample preparation, detection limits, spatial resolution, time resolution, or sample preservation. The type of information that a technique can provide about a sample is also often limited. For example, a technique might provide the chemical composition of a sample but not its molecular composition, or *vice versa*; or, it might provide molecular composition, but offer poor lateral resolution. To overcome some of these limitations, it is possible to combine two or more imaging techniques in what is called *correlative imaging*. By doing so, the strengths of a technique can complement the other and some of the limitations can be mitigated.

For example, with scanning electron microscopy (SEM) the physical topography of a sample surface can be obtained. While providing structural details at high lateral resolution, SEM by itself does not allow elemental analysis of a sample, thus, it is often combined with energy dispersive X-ray spectroscopy (EDXS); the Raman imaging and scanning electron microscopy system also combines the benefits of SEM with another technique, *i.e.*, Raman spectroscopy, which allows chemical information about a sample surface to be obtained. Transmission electron microscopy (TEM) can be correlated with

secondary ion mass spectrometry (SIMS) imaging, such that high resolution, ultrastructural TEM data can be complemented by also obtaining the chemical composition of a sample *via* SIMS; in turn, SIMS can be correlated with fluorescence microscopy to detect both the isotopic composition and optical properties of a sample.[9–11]

In the next sections, some techniques relating to MSI, EM and LM are discussed in more detail; focus will be given to nanoscale SIMS (NanoSIMS), which was the main technique used for this thesis, and to how it can be effectively correlated with EM and LM to accomplish multifaceted sample characterization.

1.2 Mass Spectrometry Imaging (MSI)

1.2.1 Overview of SIMS history

In MSI, a sample surface is hit with a primary beam (an ion or laser beam, or an electrospray), causing secondary material (*e.g.*, ions, neutral species, electrons) to be ejected. Secondary ions are extracted and directed to a mass spectrometer and separated according to the type of analyzer used. They then reach a detector, and maps of the relative intensities of each ion are generated digitally, creating an image of the sample surface which reflects the original spatial organization of its chemical identity.

Ions were discovered by Michael Faraday around 1830 through experiments of electrically charged atoms in solution, although they were only officially described by August Arrhenius in his doctoral thesis several decades later. In the late 1800s, important discoveries to the understanding of ions were made, such as the discovery of the electron and its *m/z* ratio by James J. Thomson in 1897, and the discovery that magnetic fields can change the trajectory of an ion beam by Wilhelm Wien in 1898.[12–14] The basis underlying mass spectrometry was first presented in the early 1900s by Thomson, who introduced the concept of analyzing a sample by breaking it apart into ions, accelerating them with an electric field, and separating them with a magnetic field according to their *m/z* ratio.[15] In 1913, Frederick Soddy announced that atoms of the same element could have different atomic

weights: that is, he discovered isotopes;[16] shortly after, Thomson´s collaborator Francis W. Aston built the prototype of a mass spectrometer and used it to collect a positive ion mass spectrograph and obtain the first experimental proof of isotopes.[13,17] Thereafter, several more early mass spectrometric instruments were developed, such as the ones of Arthur J. Dempster in 1922, Josef Mattauch and Richard Herzog in 1934, and Kenneth T. Bainbridge and Edward B. Jordan in 1936.[15] Meanwhile, forerunning SIMS, Woodcock and Thompson reported the production of secondary ions in 1931,[18,19] and in 1936 Arnot and Milligan used a magnetic field to separate secondary ions according to their *m/z* ratio.[20] Several advances followed, such as the first linear time-of-flight (ToF) mass spectrometry instrument providing a complete mass spectrum display built by A. E. Cameron and D. F. Eggers in 1948,[14,21] and the first coupling of a mass spectrometer with gas chromatography in 1957-9.[14,22,23] Finally, the first mass spectrometric technique applied to chemical imaging was developed in 1962 by Raymond Castaing and his student George Slodzian with the creation of the first dedicated magnetic sector instrument for secondary ion detection; the technique was called secondary ion mass spectrometry (SIMS).[24] In the 1970s and 1980s, quadrupole and ToF SIMS instrument, respectively, were designed and created.[13] Since then, several types of MSI have been developed, offering different ionization sources, as well as ion separation, focusing and detection modalities. These include techniques in laser desorption ionization (LDI), desorption electrospray ionization (DESI), and secondary ion mass spectrometry (SIMS) imaging.

1.2.2 Types of MSI: LDI, DESI, and SIMS

All MSI techniques are based off the basic principle of sputtering ions off a sample surface by hitting it with a primary beam, collecting the secondary ions, and detecting them to create images that represent the original spatial organization of the ions on the sample surface. They offer different advantages and disadvantages in sensitivity, throughput, and spatial resolution.

Laser Desorption Ionization (LDI). In LDI-MS, a laser is used as primary beam to irradiate a sample and ionize its surface, and

subsequently map the location of individual *m/z* ratio values to two-dimensional coordinates, producing images of the initial position of selected compounds on the sample surface. The first applications of LDI to mass spectrometry date back to the 1960s, and in the 1990s, matrix-assisted LDI (MALDI) was introduced by the works of Spengler and Caprioli.[25–28] The matrix used in MALDI is used to absorb energy from the primary beam and minimize sample damage, thus allowing a "soft" surface ionization to occur, *i.e.*, the surface material can be sputtered as macromolecules, preserving the molecular identity of the sample.[28] This is opposed to "hard" ionization techniques, such as dynamic SIMS, in which the ions produced are mostly atomic or diatomic. The spatial resolution of MALDI is relatively low (usually low micron resolution at best), but it offers high throughput and sensitivity for determining the mass of large analytes such as proteins, lipids, peptides and polymers.[29,30]

Desorption Electrospray Ionization (DESI). DESI builds on the concept of electrospray ionization (ESI), which is an ambient ionization technique. It was introduced in 2004 by Takas *et al.* and it is based on sputtering a sample surface at ambient conditions *via* electrosprayed aqueous charged droplets and ions of solvent, which generates secondary gaseous ions.[31] Since it can be performed at ambient conditions, DESI can be used for *in vivo* analysis and is thus suited to characterize samples in their native environment with little-to-no sample preparation. The spatial resolution of DESI is ultimately limited by the size of the droplet spray and the secondary ion transfer efficiency to the mass spectrometer; a variant, called nanospray desorption electrospray ionization (nano-DESI), features better spatial resolution (~10 μm) owing to finer capillaries and shorter probe-to-sample distance.[32] The ESI family comprises a multitude of techniques, each adapted to different analytical needs; some examples are laser ablation electrospray ionization (LAESI), probe electrospray ionization (PESI) and desorption atmospheric pressure photoionization (DAPPI). Liquid extraction surface analysis (LESA), another method similar to DESI and first described in 2010, is one such emerging imaging approach based on the use of a liquid microjunction surface sampling probe. Due to its large extraction area, the spatial resolution of LESA (typically

~1000 μm) limits its application; however, its high sensitivity and throughput have been found useful in combination with other methods.[33–35]

Secondary ion mass spectrometry (SIMS). SIMS is an imaging technique in which a sample surface is characterized *via* the detection and analysis of its molecular and elemental constituents, which are sputtered with an ion beam. It is recognized as one of the most sensitive elemental and isotopic surface analysis techniques and can be applied to a variety of solid samples as long as they can sustain ultrahigh vacuum (UHV) conditions. As already mentioned, the history of SIMS development dates back several decades. The most wide-spread early use of SIMS was in its now-called *dynamic* mode, that is, the sample surface is destroyed, and its composition analyzed as a function of depth. This found important applications in the semiconductor industry, where the layer arrangement of materials could be characterized; in fact, up to the early 1980s, SIMS was mainly used in dynamic mode. This made SIMS arguably a bulk or near-surface technique. In the late 1960s, the now-called *static* SIMS emerged through the work of the Benninghoven group, which demonstrated a non-destructive approach in a series of studies on metal oxides;[36–39] static SIMS works on the principle that hitting a sample with a very low primary ion density is non-damaging to its physical composition, and information is obtained only from the very top surface layer. This provided an operational method that made SIMS an authentic surface analysis technique. In the past several decades, SIMS instruments have seen substantial improvements, such that today it is now considered one of the most useful imaging techniques which can be applied to the analysis of a variety of sample types, boasting high sensitivity, spatial and mass resolution, and mass detection range. SIMS does come with some limitations, such as its destructive nature (in dynamic mode), challenging absolute quantification, UHV requirement, and limited spatial resolution compared to other imaging techniques.

1.2.3 NanoSIMS

Overview. In NanoSIMS, a high energy (4-16 keV) primary ion beam is rastered on a sample surface. As a result of primary ion bombardment, secondary sputtered ions are generated. Ions of a selected polarity are extracted by an electric field and accelerated into a double-focusing mass spectrometer, separated according to their *m/z* ratio, and finally they reach a detector. Intensity maps of the detected ions are computer generated and used to spatially localize the selected ions in a pixelated image. A simplified schematic of the instrument is shown in **Figure 1A**. The NanoSIMS instrument is composed of several parts: upper primary column, lower primary column, central column, coaxial column, matching optics, mass spectrometer, and multicollection system. Owing to its high mass resolution, isotopic pairs can be separated by the mass spectrometer and be detected separately at the detectors, which allows spatial localization of the enrichment of the rare isotope in the sample surface. This enables investigating the dynamics of stable isotope uptake and metabolism in biological specimens (*e.g.*, cells, tissues, plants, animals), for example, by exposing the specimen to an isotopically enriched species (*e.g.*, amino acid, drug, nutriment, air) and then localizing it in the sample in the form of isotopic enrichment relative to the natural abundance of the abundant isotope. A description of some instrumental parameters and measurement principles is provided in the next paragraphs.

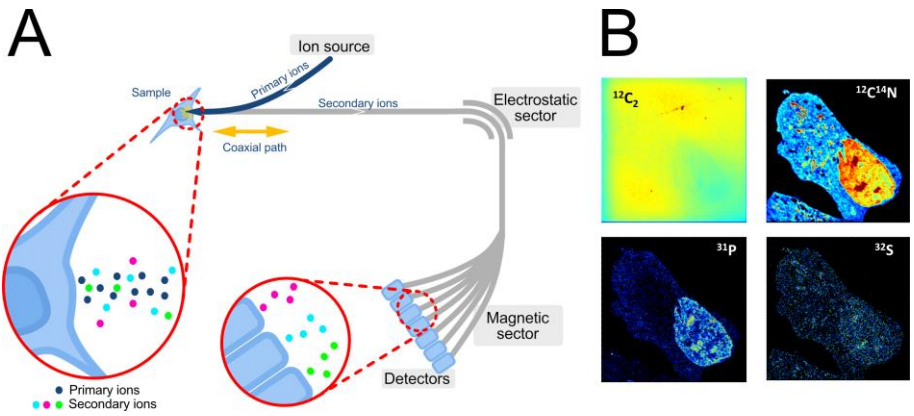

Figure 1. Simplified schematics of the NanoSIMS instrument (**A**) and examples of secondary ion ($^{12}C_2^-$, $^{12}C^{14}N$-, ^{31}P- and $^{32}S^-$) images of a neuronal progenitor cell (NPC) acquired with NanoSIMS (**B**).

Instrumentation. The first components of the instrument are the ion sources, which reside in the upper column and generate the primary ion beam. Two sources are available, *i.e.*, Cs^+ and O^- depending on the desired secondary ion polarity: Cs^+ is used when collecting electronegative secondary ions, O^- when collecting electropositive secondary ions. For the projects of this thesis, only the Cs^+ primary beam was used. In the Cs^+ source, cesium vapor is formed from a cesium carbonate pellet contained in a heated reservoir, and then ionized with a heated tungsten plate. An extraction lens directs the ions at the entrance of the lower column as an ion beam.

In the lower column, a series of electrostatic lenses and apertures shape the newly formed primary ion beam (*probe*), adjusting its current and spot size. An electrostatic Lens 1 (L1) is often used to change the probe size and current. With L1=0, the primary beam is unchanged. If a voltage is applied, a higher current is generated, corresponding to a larger probe size and higher secondary ion yield. At even higher voltages, the probe current decreases again, sometimes to a lower magnitude than the original (when L1=0); this can help achieve very low primary beam currents which will result in small spot size and high lateral resolution.[40] It should be kept in mind that lower current also corresponds to lower secondary ion yield, which can affect the counting statistics (ion counts on the minor isotope) of a measurement.

Therefore, a balance needs to be found between primary current and ion yield.[41]

NanoSIMS is a dynamic SIMS technique, so it is destructive to the sample. The so-called *static limit* is conventionally calculated as 10^{13} Cs^+/cm^2; beyond this limit, every atom on the sample surface is sputtered and sample erosion ensues; this is called *dynamic mode*.[13] Since the sample is eroded during analysis, and repeated measurements on the same sample area are not possible, the secondary ion signal needs to be optimized in order to have enough sample material arriving at the detectors. The NanoSIMS ion optics are optimized to enhance the transmission of the instrument, *i.e.*, the fraction of starting sputtered ions over the ions arriving at the detectors.

The NanoSIMS features a coaxial configuration whereby the incidence path of the primary ion beam is orthogonal to the emerging secondary ion beam (**Figure 1A**, *coaxial path*); this ensures the shortest possible distance between the sample surface and the extraction lenses, which enhances secondary ion collection. After sputtering and ion extraction, a transfer optical system (lenses, deviating plates, apertures) shapes the beam to minimize aberrations and further optimize transmission. For example, in the central column, a set of deviating plates, which control the rastering of the primary ion beam and keep the beam in the center of the final field diaphragm (D1), cancel the motion of the secondary ion beam at the entrance slit (ES) to the mass spectrometer. This increases the transmission of the instrument by ensuring as many secondary ions as possible enter the mass spectrometer.

Mass resolution in mass spectrometry imaging is defined as the ability to separate secondary ions that differ in *m/z* ratio, and is defined as $M/\Delta M$, where M is the mass of the ion of interest and ΔM is the difference in mass between the ion of interest and the adjacent ion.[13,42,43] High mass resolution in NanoSIMS is achieved by the use of a Mattauch-Herzog mass spectrometer, named after the two scientists who developed it in 1934.[44] It is also called a double-focusing mass analyzer, because it comprises two parts: the first part is an electrostatic sector, which filters the secondary ions according to their kinetic energy; the second is a magnetic sector, which focuses them based on

their *m/z* ratio. This allows ions of a given *m/z* ratio which have different starting kinetic energy to be focused to a focal point.[13] This configuration finds excellent applicability in the NanoSIMS, where the energy spread of the secondary ions is large (0-2000 eV) and allows transmission of a high fraction of sputtered ions (up to ~40%). Isobaric (mass) interferences can also be overcome. These interferences can be a significant issue in mass spectrometry and appear when two ions have the same nominal *m/z* ratio and arrive at the same detector. Owing to the high mass resolving power of NanoSIMS, isobaric species can often be separated, allowing accurate results.[13]

The secondary ion beam finally reaches the multicollection system. The NanoSIMS features seven trolleys, each equipped with an electron multiplier and a Faraday cup (FC). In imaging mode, electron multipliers are used as they have faster response time compared to FCs; FCs have higher sensitivity and are sometimes used for precise quantitative ratio measurements.[45] A set of parallel plates also corresponds to each trolley and these are used to scan the mass line and obtain a so-called *high-mass resolution* graph, which is used during tuning to center the desired mass at the corresponding detector. The electron multipliers receive the secondary ions one by one and generate a signal in the form of current, which corresponds to the intensity (number) of incoming ions. Intensity maps for each ion are then created (*e.g.*, **Figure 1B**) and localize the chosen ions and their relative abundance in each pixel of the image.

Measurement principles. The yield of secondary ions in the NanoSIMS depends on a number of parameters. The basic SIMS equation is:

$$I_s(A) = I_p \cdot Y \cdot \alpha(A) \cdot c(A) \cdot T$$

where $I_s(A)$ is the secondary ion beam current for species A, Ip is the primary ion beam current, Y is the total sputter yield, α(A) is the ionization probability of species A, c(A) is the fractional concentration of species A in the matrix, and T is the transmission of the instrument.[46] The equation states the relationship between the secondary ion current and the concentration of the species of interest in the sample. The so-

called *matrix effect* emerges as one of the terms is the ionization potential of the species, which changes according to the bulk composition of the sample. The matrix effect describes the variation in secondary ion yields, which can span several orders of magnitude, depending on the composition of the sample from which the ions are generated. This effect is often significant and unpredictable; therefore, it is the reason why absolute quantification in NanoSIMS can be problematic.[13] In order to carry out absolute quantification, calibration standards having the same matrix as the sample of interest must be produced.

Secondary ion signal is not stable at the beginning of a NanoSIMS measurement; the variations in secondary ion signal that occur during the initial stages of sputtering (*transient state*) are referred to as the *transient effect*. A so-called *steady state* of sputtering is achieved after a certain amount of Cs^+ ions are implanted to the sample surface; this process is called *implantation*. During implantation, secondary ion sputtering is enhanced, and this enhancement scales with the concentration of Cs^+ implanted into the sample surface. The oscillations of sputtering yield as a function of positive primary ion bombardment are a longstanding topic and have been described extensively.[47–51] Steady state refers to the state where the primary ion implantation rate compares to the sputtering rate of implanted primary ions, *i.e.*, an equilibrium is reached between primary ions and sputter rate. The sputter-enhancing effects of implantation are predominantly attributed to changes in work-function/ionization potential of the sample surface.[13] Performing measurements at steady state is recommended when high sensitivity is required (*e.g.*, small differences in isotopic enrichment are being monitored), or when carrying out absolute quantification.[40,52]

In imaging, the term *spatial resolution* describes the minimum distance needed to resolve objects in an image. Spatial resolution in SIMS is defined as the ability of the instrument to separate signals from two adjacent locations and is usually taken as the distance over which a secondary ion intensity at an abruptly changing signal (*e.g.*, the edge of a cell or cellular feature) drops from 84% to 16% (this is called the *16-*

84% criterion).[10,13] The NanoSIMS can reportedly provide a lateral resolution down to 50 nm. In practice, this is not easily achieved as there are many factors which can influence the resolution of an image other than the parameters of the instrument, such as the composition of the sample (*e.g.*, topography, density) and the time available for analysis (high pixel resolution can make a measurement very time intensive). Some of the instrumental parameters that control the final image resolution are the primary beam current, the size of the D1 aperture, the pixel resolution, and the sputtering dwell-time. Resampling (*e.g.*, oversampling and undersampling) can also affect lateral resolution. Oversampling occurs when the size of the primary beam is larger than the pixel size of the image, such that some parts of the sample surface are probed more than once, and the secondary ion yield is increased. An interpretation of this is illustrated in **Figure 2**, which also shows how the effect of beam mixing can affect resolution. Beam mixing occurs when adjacent features in a sample are probed at the same time by a large primary beam, and do not get resolved separately. This can cause signal dilution and poor lateral resolution. This effect can be reduced by using a smaller beam and higher pixel resolution.

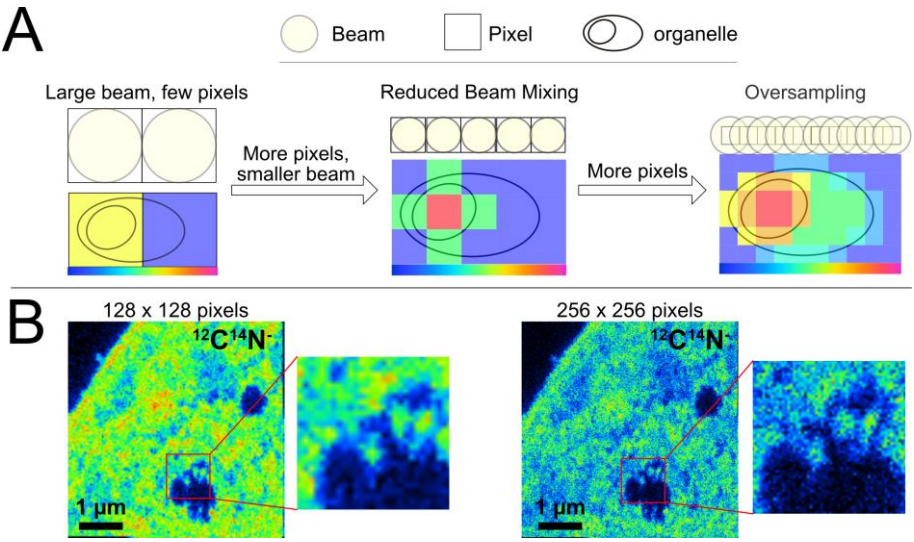

Figure 2. Schematics of how beam mixing and oversampling can improve lateral resolution (**A**) and an example $^{12}C^{14}N^-$ image of an NPC imaged with identical instrumental parameters except pixel size (**B**), where the image on the right is more oversampled and appears more resolved.

Data analysis. NanoSIMS can be used to quantify the isotopic enrichment of elements in a sample. In biological samples, this can be useful when investigating the biological pathways and dynamics (*e.g.*, uptake, turnover) of molecular species. Once intensity maps for an isotopic pair are acquired, relative enrichment (δ) of the rare isotope can be expressed in per mille (‰) as:[53]

$$\partial‰ = \frac{R_{sample}}{R_{standard}} \times 1000 - 1000$$

where R_{sample} is ratio of the sample in a region of interest (ROI) and $R_{standard}$ is the natural abundance ratio of the element. For elements which are being measured directly and not as isotopic enrichment (*e.g.*, halogens, transition metals), their enrichment can be normalized against a homogeneous background ion in the sample (for example, for resin embedded samples containing carbon, they can be normalized against $^{12}C_2$).

The analytical precision of a NanoSIMS measurement is largely dependent, on a fundamental scale, by the so-called *counting statistics*, which limit the precision achievable under ideal instrumental circumstances. The counting statistics are dictated by Poisson statistics, in the way that secondary ion counts at the detectors approach a Gaussian distribution as the number of counts increases. For any δ, a Poisson uncertainty in per mille can be calculated as:

$$\text{Poisson uncertainty (‰)} = \frac{1000}{\sqrt{\text{area (pixels)} \cdot \text{Num}\left(\frac{\text{counts}}{\frac{\text{seconds}}{\text{pixel}}}\right) \cdot \text{dwell time (s)} \cdot \text{number of cycles}}}$$

where area (pixels) is the area of the ROI from which the δ is taken, Num (counts/seconds/pixel) is the counts on the rare isotope (the counts on the abundant isotope can be usually omitted as they are often very high), dwell time (s) is the counting period at each pixel, and number of cycles is the number of planes/cycles acquired during the measurement.[54] If the Poisson uncertainty is high (a definition of a high uncertainty will be somewhat arbitrary and relative to the measured

enrichment), the measurement is not reliable; for a given sample with a set enrichment, the uncertainty increases with smaller ROIs, lower dwell time, and fewer number of cycles.

Other sources of error and uncertainty need to be considered during NanoSIMS data analysis. Images usually need to be dead-time corrected: the dead-time is the time during which an EM is "blind" to an arriving ion because it has not finished recording the previous one, leading to an underestimation of the signal. In NanoSIMS, the dead time is 44 ns and can be corrected for automatically by most image analysis software. Quasi-simultaneous arrival (QSA) is another underestimating factor. QSA occurs when two ions are ejected from the sample surface by one impinging primary ion, thus arriving at the detector simultaneously and being recorded as a single ion.[55] QSA can sometimes be corrected for by choosing to detect a similar ion with a lower ionization potential in a certain substrate (for example, detecting $^{12}C^-$ instead of $^{12}C_2^-$, or *vice versa*) or by mathematically correcting for it.

1.3 Microscopy

1.3.1 Overview

As with most analytical imaging methods, microscopy involves the study of objects that are too small to be seen with the naked eye. The way we see our surroundings and the ability to interpret the visual world around us is innately limited by the way we can perceive it at a physical level. Our eyes capture and focus light from the objects around us and our brain interprets it. Overall, the visual process is restricted by our ability to resolve objects. Therefore, anything which is smaller than the limit of resolution of our eyes remains entirely unknown. In addition, our eyes are only sensitive to light in the visible region of the electromagnetic spectrum, *i.e.*, 400-700 nm in wavelength (λ). Being able to "see" things beyond these limits was ultimately achieved after scientific developments that lasted millennia, starting with the emergence of rudimental Greek optics and building up to the variety of ultrahigh-resolution imaging techniques which are available nowadays. Different microscopy categories exist, according to the type of source

used to generate the image (electron, light and scanning probe microscopy). The term *optical* microscopy also refers to the use of visible light to create an image.

1.3.2 Types of Microscopy: EM, LM and SPM

Microscopy techniques are based on how different sources (*e.g.*, electrons or light) interact with a sample and how these can be used to image samples. Several parameters relating to the quality and stability of an imaging system can affect the resolution of a microscopic image, but the most determining factor is the wavelength of the imaging medium. In general, the smaller the wavelength, the higher the resolution that can be achieved; thus, the wavelength used determines the minimum size of an object that can be distinguished with a certain technique. In microscopy, the final resolution of an image is given by $r = \lambda/2$, where r is the resolution and λ is the wavelength. In light microscopy, λ is 400-700 nm (the wavelength of visible light), therefore the highest resolution that can be achieved by conventional techniques is 200 nm; electrons, on the other hand, have a much smaller wavelength and can theoretically provide resolution under 2 pm. The principles underlining different microscopy techniques are varied; they have different requirements in sample preparation and instrumentation and provide different parameters in resolution and sample information. Some of them are discussed next.

Electron microscopy (EM). The first prototype of an electron microscope was built by Ruska and Knoll in 1931, and has since been established as one of the imaging techniques providing the highest spatial resolution.[56] In EM, an electron beam is directed at a sample surface using an accelerated potential. Since they are negatively charged, electrons can be focused using electric or electromagnetic fields, similarly to ions. The main parts comprising an electron microscope are an electron source (often a tungsten filament) and focusing lenses and apertures which direct and shape the beam. When electrons interact with a sample, different species can be generated, such as secondary electrons, photons, and radiation; the former can be used to form an image. Depending on the type of technique, the primary electrons can be made to either pass through the specimen or be

reflected and backscattered; these approaches are called transmission electron microscopy (TEM) and scanning electron microscopy (SEM), respectively. TEM is further described in section *1.3.3 Transmission Electron Microscopy (TEM)*.[57]

Light microscopy (LM). Light microscopes were invented in the early 1600s, building on the development of optics which encompassed theories from the ancient Greek and Arab scholars, and slowly gained interest among European scientists. Antoine van Leeuwenhoek, a Dutch draper-turned-microscopist, is generally attributed the invention of the first microscope, although others, such as Galileo Galilei, Hans Janssen, and Cornelius Drebbel, are also regarded as having built simple and compound microscopes around the same time.[57–59] In LM, a light beam is used as primary beam to image a sample. The properties of the primary light source, such as wavelength, polarization, and angle of incidence, can be different and generate different results. Several types of LM exist, such as bright field, dark field, phase contrast, and fluorescence microscopy; the latter is further described in section *1.3.4 Confocal and Stimulated Emission Depletion (STED) Microscopy*.

Scanning probe microscopy (SPM). The first SPM image was created in 1981, after the first SPM device, a scanning tunneling microscope, was conceived and built by Gerd Binnig and Heinrich Rohrer.[60] In SPM, a sharp pointed tip ("probe") is raster-scanned very close to a sample surface, and feedback signals of the sample-probe interactions are used to create an image. Different types of SPM are in use, and these include atomic force microscopy (AFM) and scanning tunneling microscopy (STM). In STM, a voltage is applied between sample and probe so that electrons can travel between the two *via* the phenomenon of tunneling. STM offers good spatial resolution (down to 0.01 nm) and is a non-destructive technique. Some limitations include the impossibility for bulk analysis (SMP is inherently a surface analysis technique) and the need for conductive or semi-conductive samples. AFM, on the other hand, works by detecting local mechanical forces through a cantilever and using them to image a surface, and can image almost any type of sample, without being restricted by their conductivity.[61]

1.3.3 Transmission Electron Microscopy (TEM)

Overview. In TEM, an electron beam is passed through a thin sample to create an image. The beam is shaped by apertures and lenses and arrives at the sample surface in a tightly focused spot, interacts with the atoms in the sample, and generates an image based on their arrangement. Owing to its high lateral resolution, TEM is one of the best-suited techniques for investigating the fine ultrastructure of biological samples. A schematic of a TEM instrument is presented in **Figure 3**, showing some of the main components of the instrument. An overview of TEM concepts is discussed in the next paragraphs; sample preparation for TEM imaging is further discussed in *Chapter 3*.

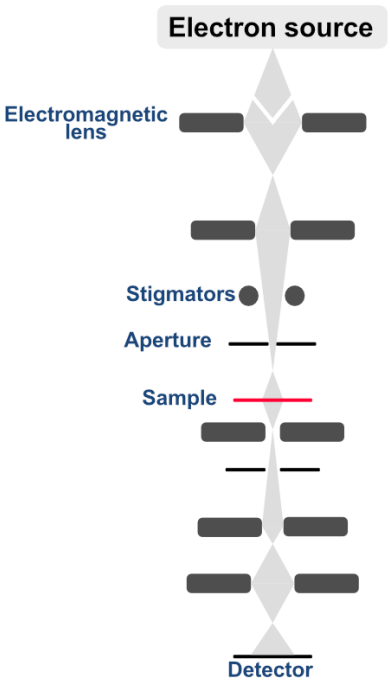

Figure 3. Simplified schematic of a TEM instrument.

Electron optics and image formation. TEM involves the manipulation of an electron beam using a series of electromagnetic lenses. When the electron beam passes through an electromagnetic lens in a TEM instrument, it is bent (focused or defocused) to a desired size according

to the strength of the magnetic field. By combining subsequent lenses and apertures in its path, the beam is made to arrive to a small spot on the sample surface. Other optics components, such as stigmators and deflectors, regulate symmetricity and tilt of the electron beam to ensure optimal beam shape. Once it arrives at the sample, the beam penetrates it, and the transmitted electrons are detected by a camera positioned below the sample. Denser or thicker sample regions scatter the electrons in the beam more than lighter ones; therefore, atoms with larger molecular weight scatter the electrons in the beam more than lighter ones. This is why biological samples are usually stained with heavy metals in order to improve the contrast of the image (this is further described in *Chapter 3*). The scatter generates a diffraction pattern that is used to automatically reconstruct an image of the sample. A greyscale projection is obtained corresponding to the atoms in the sample, with areas where there are heavier atoms corresponding to darker regions in the image, and areas with lighter atoms corresponding to lighter regions.

Lateral resolution. The highest resolution achievable with an optical image forming system is given by the Rayleigh criterion, which sets a fundamental limit to optical resolution: $r = (0.61\lambda)/NA$ where r is the resolution, 0.61 is a constant, λ the wavelength, and NA the numerical aperture. Simply stated, from this equation, the ability of the system to resolve objects that are close to each other, *i.e.*, at a small angular distance, is commonly limited by the wavelength of the imaging medium and the numerical aperture of the system. Thus, with a given optical system with a set NA, the resolution of a microscopic image is dependent on the wavelength of the medium which interacts with the object being observed.[57] Smaller wavelengths lead to higher resolution.

As mentioned, visible light has a wavelength between 400-700 nm. While this limit can be challenged with the use of super-resolution approaches, it sets an underlying restraint to the highest resolution achievable with optical microscopy. Electrons, on the other hand, also possess a wave-like character; the De Broglie equation describes their wavelength as: $\lambda=h/p$ where h is the Planck constant, and p is the momentum (mass times speed) of the electron. Since the mass is

constant, the wavelength of an electron depends entirely on its speed, with higher speed corresponding to shorter wavelength.

Accelerating electrons, focusing them, and passing them through a thin sample generates an image. Because very short wavelengths can be achieved (*e.g.*, with an accelerating voltage of 120 keV, the velocity is $\approx 2 \times 10^8$ m/s and $\lambda \approx 0.004$ nm), the theoretical image resolution can be very high. Using an approach of image formation similar to optic systems, the theoretical image resolution can be calculated as $r = 0.61\lambda/(n \cdot \alpha)$, where n is the medium refractive index (1 for TEM since the medium is vacuum) and α is the convergence angle;[62] thus, assuming $\alpha = 0.01$ radians, the theoretical resolution of a TEM image with a 120 keV beam is around 0.2 nm.

Yet, when imaging biological samples, the resolution can be limited by several factors other than the electron wavelength, such as sample preparation, radiation damage, and aberrations.[63] For example, sample preparation often includes staining of biological membranes with heavy metals, which bind to proteins and/or lipids; this affects the resolution because the stain creates a uniform appearance of the ultrastructural feature, regardless of its thickness. In TEM, thin samples (*e.g.*, commonly 70-300 nm in thickness) are necessary to allow the electron beam to penetrate the sample during the imaging process. However, very thin samples are vulnerable to damage from exposure to the high-energy electron beam; this can ultimately spoil the sample and result in change in specimen structure.[57,64] Furthermore, aberrations such as spherical or chromatic aberrations and astigmatism can lower the image quality; these can be corrected to a certain extent (*e.g.*, properly calibrating the instrument before and during imaging), but they are sometimes intrinsic to the physis of the instrument and can maintain a residual impact on the final image resolution. Additionally, while theoretically improving the resolution, higher voltage decreases image contrast because electrons pass through the sample more efficiently and this can also affect the image quality. Thus, the resolution of a TEM image of a biological sample depends on several factors, nonetheless it remains excellent for the purpose of resolving nanometer-scale subcellular features such as membranes and organelles.

Artifacts and image interpretation. While 3D imaging is possible with TEM (*i.e.*, tomography) using specialized equipment and software, conventional 2D TEM imaging only provides a flat representation of a sample. Understanding the nature of a two-dimensional image is important to avoid misinterpreting the different structures visible in a biological sample (*i.e.*, a tubular organelle might appear round if the sectioning plane is perpendicular to it). Understanding the different sources of contrast and how they affect the image is another important point for accurately interpreting TEM images, since contrast is often artificially introduced to biological samples with the use of heavy metal stains. These can cause artifacts due to improper sample preparation (*e.g.*, heavy metal precipitation) or, as discussed, block out microstructures or minute sample features if they are stained uniformly to the surrounding structure (*e.g.*, a membrane bilayer can appear as a monolayer). In fact, a large number of artifacts can be encountered in TEM, which can be formed during the sample preparation (preparation-induced artifacts) or during the imaging of the sample (observation artifacts). Preparation-induced artifacts include mechanical damage (*e.g.*, deformation and tearing) and change to the sample structure due to chemical or physical reactions. Observation artifacts include beam misalignment (*e.g.*, shading) and thermal damage (beam damage), such as charging effects and sample destruction.[65] These can be avoided with proper sample preparation and handling and operation of the instrument. Some examples of artifacts are shown in **Figure 4**.

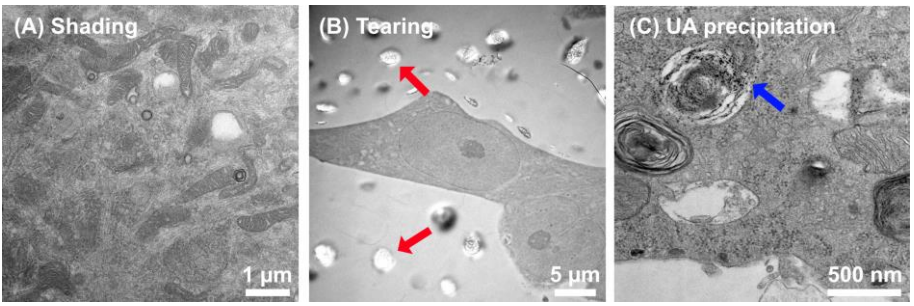

Figure 4. Examples of artifacts in TEM imaging. (**A**) Shading caused by improper beam alignment. (**B**) Tearing possibly caused by improper sample handling during or after ultrathin sectioning (red arrows). (**C**) uranyl acetate (UA) precipitation due to inadequate sample preparation (blue arrow).

Advantages and limitations. TEM is a versatile technique that can be applied to a range of applications, including biology, materials science, and medicine. The principal advantage of TEM is undoubtedly the spatial resolution that it provides. For biological samples, TEM allows the study of the ultrastructural details of cells and tissues, and even to go down to single proteins and small molecular complexes. The technique does present some disadvantages and limitations. These include cumbersome and labor-intensive sample preparation, limitation to fixed and ultrathin samples, and relatively slow throughput. While possible with some approaches (for example when used in hybrid mode with some spectroscopy techniques, or with the use of specific labeling strategies),[66–68] conventional TEM also fails to provide the chemical composition of a biological sample, instead only providing structural information. For this reason, it is often correlated with other imaging techniques such as LM and SIMS.

Correlation with NanoSIMS. TEM is often used in correlation with MSI techniques. This is because mass spectrometry images provide the chemical (molecular or atomic) composition of a biological sample, but little to no ultrastructural information. For example, TEM finely resolves organelles such as secretory vesicles and mitochondria, but these appear in NanoSIMS as more-or-less carbon and nitrogen (detected as $^{12}C^{14}N^-$) dense regions, which blend in with the surrounding cellular space. An example of this is shown in **Figure 5**. By imaging the same sample area with TEM and NanoSIMS, both structural and compositional information can be obtained, allowing for a more comprehensive understanding of a sample.

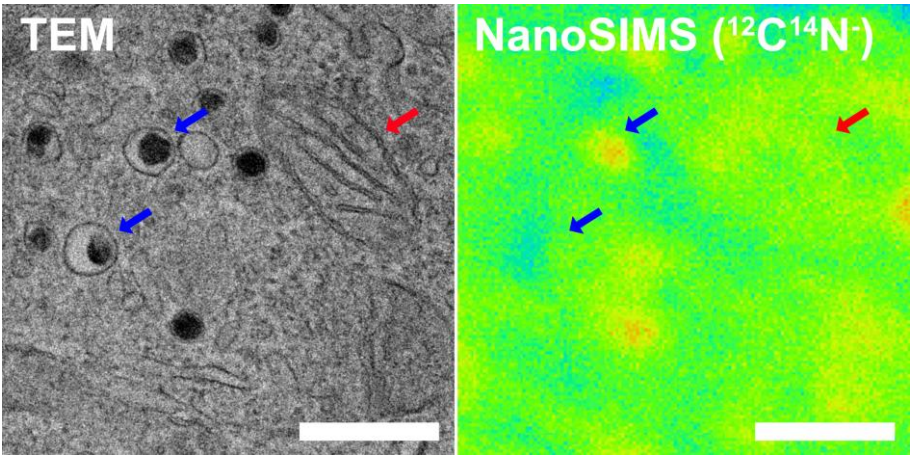

Figure 5. Example of TEM and NanoSIMS image correlation. The same PC12 cell is imaged with both techniques: the TEM image provides ultrastructural information and localizes organelles such as vesicles (blue arrows) and mitochondria (red arrow), while these are not discernible in the NanoSIMS image. By overlaying the two images, every organelle can be characterized by their compositional ($^{12}C^{14}N^-$) content. Scale bar is 500 nm.

1.3.4 Confocal and Stimulated Emission Depletion (STED) Microscopy

Overview. The way that light is used to produce an image in LM is conceptually similar to the way electrons are used to produce an image in EM. That is, the beam is passed through a series of beam-shaping lenses, arrives at the sample, interacts with it, and generates information about the sample which a detector uses to form an image. As mentioned, the fundamental resolution limit in optical microscopy is about 200 nm, but advances in the field have significantly extended this limit with what are now called super-resolution techniques. STED is one such improvement and is discussed in the next paragraphs together with conventional confocal microscopy.

Confocal and STED are two types of fluorescence microscopy (FM). In FM, a light beam (*e.g.*, a laser) is directed at a sample containing a fluorescence tag (*i.e.*, a molecule which is introduced in a sample and attaches to specific biomolecules); during imaging, the photons from the beam interact with the tag, which absorbs some of the incoming energy and then releases secondary photons. Because some energy is lost in this process, the generated photons have lower energy and thus

longer wavelength than the incident ones. A detector is tuned to receive this emission wavelength, and an image is created which reveals the intensity of the arriving photons as a function of their location in the sample.[69]

Instrumentation and optics. A fluorescence microscope comprises a primary light source, a series of refractive lenses, and a detector. The lenses are used to direct the light at a sample; in confocal and STED microscopy, a set of scanning mirrors raster the light beam onto the sample surface, and each raster spot is represented by a pixel in the final image. A dichroic filter acts as a beam splitter and separates the excitation and emission light. The beam splitter does this by reflecting light of a selected wavelength towards the sample, whereas the light emitted from the sample is transmitted towards the detector.[69] A schematic of a confocal/STED microscope is shown in **Figure 6**.

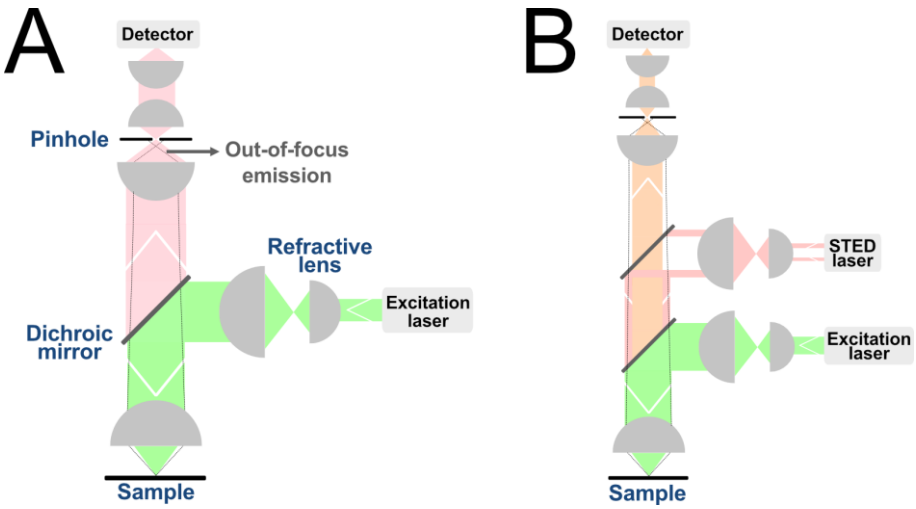

Figure 6. Simplified schematics of confocal (**A**) and STED (**B**) microscopes.

Confocal *vs* STED. In confocal microscopy, a laser light beam is rastered on a thin (*e.g.*, cell monolayer) sample, exciting fluorophores which emit fluorescent light. The laser is tuned to a specific wavelength corresponding to the excitation spectrum of the fluorophore of interest. The emitted light is directed through a pinhole which blocks out-of-focus light, allowing only in-focus light to reach the detector; this enhances the resolution by generating a sharper final image with more

contrast. The use of the pinhole is one key difference between confocal and widefield microscopy, in which a sample is uniformly illuminated, and all emitted light detected.

STED microscopy was developed in 1994 by Stefan W. Hell and Jan Wichmann,[70] and has been gaining momentum owing to its improvements in spatial resolution compared to conventional microscopy techniques. It uses two lasers: one for excitation and one for depletion (*STED beam*). The STED beam is shaped into an annular shape (commonly referred to as the "donut" shape) and is emitted immediately (within a few nanoseconds) after the excitation beam at a different (typically shorter) wavelength; its role is to force the fluorophore back to its non-excited state and therefore deplete it before it emits fluorescent light, consequently only letting the non-depleted fluorophore emit light from the complementary region. This reduces the size of the focal spot and improves lateral resolution, which can be in the range of tens of nanometers.[71] A simplified schematic of the STED beam is shown in **Figure 7**.

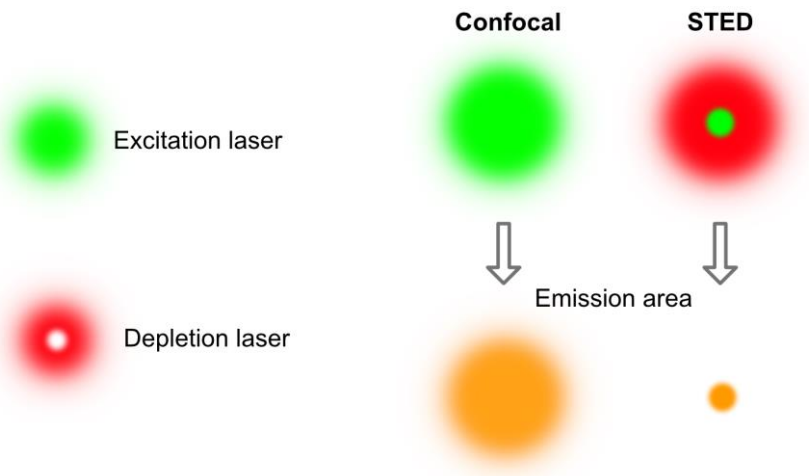

Figure 7. Schematic of the difference between confocal and STED lasers. While the confocal laser excites all the fluorophores in the area, the depletion (STED) laser additionally quenches the fluorophore in the annular region, only letting emitted light emerge from the complementary area.

Labeling strategies. There are different approaches to label molecules for FM. These generally include antibody, genetic, and dye labeling

(*staining*). The choice of labeling method depends on the research question and experimental design of a specific study.

Antibody labeling, also known as immunofluorescence staining, involves the binding of antibodies to specific biomolecules in cells and tissues. The antibodies recognize and bind to a target molecule. Two types of antibody labeling are possible: direct and indirect. In direct labeling, the antibody is directly conjugated to a fluorophore (this is known as a *fluorochrome*) and can be imaged directly using FM. This approach is sometimes preferable as it is easier and faster, as long as a suitable fluorochrome is available. For indirect labeling, the antibody is not directly labeled; instead, a secondary antibody, conjugated to a fluorophore, is used to bind to the primary one. This approach is more versatile, as a wide range of commercially available secondary antibodies exist that can be easily matched to the primary antibody according to the host species from which it is derived. Finally, when imaged using FM, the fluorophore in the antibody (whether primary or secondary) allows an image of the spatial distribution of the target molecule in the sample to be generated.[72]

Genetic labeling is another popular approach to labeling in FM. This involves the insertion of a fluorescent protein gene into a living biological substrate (*e.g.*, cells) to stimulate the expression of fluorescent molecules. This allows visualization of specific structures in cells which are tagged with the genetically modified species introduced in the substrate. Many fluorescent proteins have been identified and are available today. For example, a cell might be engineered to express a green-fluorescent protein (GFP) in place of a non-fluorescent protein. GFP was the first fluorescent protein discovered, purified from *Aequorea Victoria*, a type of jellyfish, by Osamu Shimomura in the early 1960s.[73,74] During FM, the GFP emits light when excited by the appropriate wavelength, which can localize cellular structures which contain the fluorescent protein. Genetic tagging is particularly useful for long-term, stable labeling of living samples.[72]

Staining is typically less specific than antibody and genetic labeling, but it can be easier and/or cheaper to perform. Staining involves the

selective chemical binding of a fluorescent dye, also called chemical fluorescent probe, to a biological structure. Different dyes can selectively stain different components in a cell, such as the nucleus, membrane, and cytoskeleton. The specificity of binding depends on the chemical properties of the dye. Some dyes may require cell membrane permeabilization and can only be used on fixed samples, but some cell permeable dyes are available which allow for live imaging. Many different dyes can be commercially purchased for different biological structures, and can be chosen according to the desired specificity, emission wavelength, and permeability.[72]

Advantages and limitations. One advantage of confocal and STED microscopy is the lateral resolution, which is especially enhanced in STED. A great advantage of FM is that is can often be performed *in vivo*, because it does not require a vacuum. Thus, physiological and chemical phenomena can be tracked in living biological samples, and time-lapse images can be recorded and composited into time-lapse videos. Additionally, relatively thick (a few μm) samples can be imaged with good contrast and resolution, and 3D imaging is possible by acquiring images in stacks and later combining them into 3D images with a software. Since it employs two lasers instead of one, STED microscopy has lower temporal resolution than confocal microscopy, which can sometimes limit its applicability (especially in live-cell imaging). Photobleaching is also a disadvantage for both techniques and can cause loss of signal during sample handling and imaging. The use of tags (*i.e.*, dyes and antibodies) can also cause image displacement, in which the original position of the labeled structure is shifted compared to that of the signal, because of the size of the tag; this can sometimes be mitigated by the use of smaller tags (*e.g.*, nanoprobes).

Correlation with NanoSIMS. FM can efficiently be correlated with MSI techniques. While NanoSIMS provides the chemical composition of a sample surface, FM can spatially localize labels and stains which reveal the biological identity of a target. For example, an organelle or a molecule in a cell can be labeled and imaged with confocal microscopy, which will provide an image of their arrangement in the cell as a

function of their optical interaction with the primary light beam. An example of this is shown in **Figure 8**. Here, the Ras GTPase-activating protein-binding protein 1 (G3BP1) protein in stress granules (further discussed in *Chapter 4*) in a neuronal progenitor cell (NPC) is labeled with the anti-G3BP antibody and secondary antibody STAR 635, and the nucleus is stained with the dye DAPI. Correlation of FM and NanoSIMS can be useful to localize a specific target in a biological sample using FM and obtaining its chemical composition using NanoSIMS.

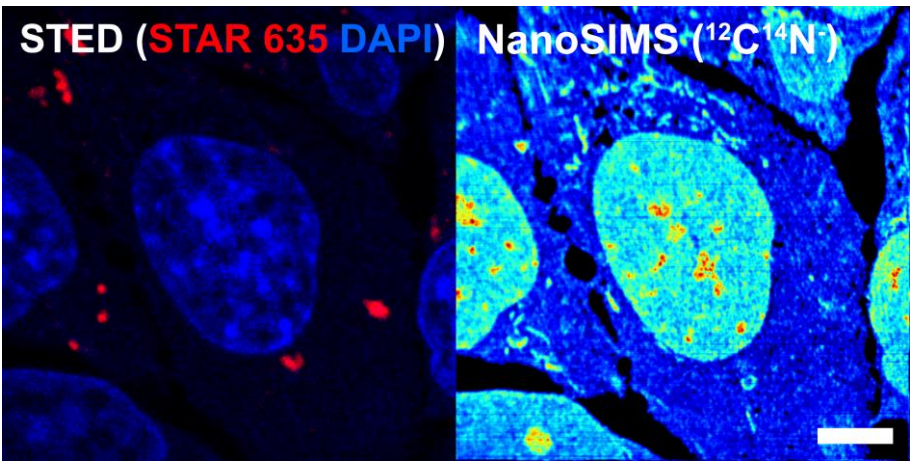

Figure 8. Example of STED and NanoSIMS image correlation. The same NPC is imaged with both techniques: the STED image localizes organelles (stress granules, red, and nucleus, blue) in the cell, while NanoSIMS obtains the compositional ($^{12}C^{14}N^-$) information. Scale bar is 5 μm.

Overall, choosing the best analytical technique for a type of sample requires considering the differences in principles and output that each technique provides; correlative imaging allows the combination of two or more imaging methods in order to mitigate the limitations and strengthen the advantages of individual techniques, leading to more comprehensive sample characterization. When approaching a specific research question in correlative chemical imaging, it is further necessary to acknowledge the type of biological system to be used, and the most suitable sample preparation available to devise an optimized protocol. Some of these aspects are discussed next.

CHAPTER 2. Biological Systems Imaged in this Thesis

2.1 Overview

Cellular and molecular biology involves studying the characteristics and interactions of biological systems, and the structures and mechanisms underlying biological processes. Cells are a fundamental part of modern biology, and by understanding how cells function at a molecular level, many life processes such as cell growth, division, metabolism, differentiation, and development can be elucidated. This can also offer insights into how organisms respond to external inputs such as environmental and chemical stimuli, and even provide the tools to understand and treat diseases.[75] Moreover, biology can intertwine with chemistry, as cells can be used as models systems to study the interplay between chemical and biological processes.

Different types of samples can be studied in biochemistry. For example, clinical biochemistry deals with the detection and measurement of chemicals in bodily fluids, for instance blood, saliva, urine, feces, cerebrospinal fluid, and sweat, to diagnose and monitor diseases in patients using analytical methods such as flow cytometry, electrophoresis and spectrometric techniques.[76,77] In fundamental biochemical research, a variety of samples can be used, including cells, tissues, organoids and biochemical molecules (*e.g.*, isolated proteins). For the work that is included in this thesis, single cells were employed and are thus the focus of this chapter.

In this thesis, *single cells* refer to cells which have been isolated and are cultured separately *in vitro*. Single cell analysis is an important tool in biochemistry as it provides information about the characteristics (*e.g.*, cell heterogeneity, signaling pathways, molecular components) of cells and how these differ between different cell populations.[78] The type of cell model used in single cell analysis is dependent on the research objective; for example, for the study of a specific disease, a cell model that closely mimics the diseased cells may be selected. Some of the

main categories of cell models are immortal cell lines, primary cells, and stem cells.

Primary cells are harvested directly from a tissue explant. They have a limited lifespan, as they have limited capacity to proliferate.[79] This is known as *Hayflick limit*, after Leonard Hayflick who first discovered this phenomenon in the 1960s.[80,81] In a series of experiments on human fibroblasts, he showed that the cells could only replicate a finite number of times, after which division stopped and the cells eventually died. This challenged the dogma that all cells could divide indefinitely and introduced the limit as a fundamental difference between cultured cancer cells and primary cells. The Hayflick limit does not relate to the passage of time, but instead to rounds of DNA replication, and therefore the number of population doublings (*passages*).[79]

One of the most widely used human primary cell types is the hepatocyte, which is used to test for drug susceptibility to metabolism and hepatotoxicity. Brain derived neurons have also been used to study signaling and changes in response to drugs.[82] Primary cells can be more relevant than immortal cell lines in the investigation of therapeutic targets in drug screening, as their phenotype is more similar to that of the *in vivo* cells from which they are derived. Nonetheless, they have limited use in long-term experiments due to the Hayflick limit, and may require specific culturing conditions (*e.g.*, specialized growth factors or substrates) which can make their maintenance more challenging and expensive.

The cellular models employed for the work included in this thesis are of two other kinds: an immortal cell line (pheochromocytoma 12, PC12) and stem cell-derived cells (neuronal progenitor cells, NPCs).

2.2 Immortal Cell Lines and Pheochromocytoma 12 (PC12) Cells

While animal cells have been cultured *in vitro* since the 1900s, the first immortal cell line, mouse L cells, was reported in the 1940s.[83] The first human immortal cell line created was the HeLa line, isolated in the

1950s by Dr. George Gey and colleagues from a tissue sample of a cancer patient named Henrietta Lacks.[84] Since then, many more lines have been created and are used widely in laboratories across the world. Immortal cell lines are generally inexpensive, stable, and relatively easy to handle. They replicate indefinitely, so they can be used repeatedly for experiments, and many are commercially available. Furthermore, using immortal cell lines offers a means to study cellular processes *in vitro* and minimize the use of live animals in research.[85]

Immortalizing cells can be achieved by various techniques, such as *via* exposure to irradiation, carcinogens, oncogenes, and viruses.[85,86] Immortal cells are used as model systems to study diseases and for drug discovery and development; additionally, they can be used to produce biomolecules for biotechnological and medical applications. While they are useful in a variety of applications, it is important to note that they might not always reflect the behavior of cells *in vivo*, making them less physiologically relevant compared to other types of models. Nevertheless, they remain excellent for preliminary investigations and screenings, given their robustness and ease of use.[82] Some common immortal cell lines include HeLa, CHO (Chinese Hamster Ovary cells), HEK 293 (Human Embryonic Kidney cells), MDCK (Madin-Darby Canine Kidney cells), MCF-7 (breast cancer cells), and Vero (green monkey kidney epithelial cells).

Pheochromocytoma 12. PC12 cells are an immortal cell line commonly used in the study of neuronal communication and differentiation. They were first isolated in 1976 by Lloyd Greene and colleagues[87] from a rat (*Rattus norvegicus*) pheochromocytoma (neuroendocrine tumor) of the adrenal medulla (*intra-adrenal paraganglioma*).[88] The pheochromocytoma is a tumor composed of adrenal chromaffin cells that overproduce catecholamines. PC12 cells mainly synthesize, store and release dopamine as a neurotransmitter, and sometimes small amounts of norepinephrine, and their release is calcium-dependent.[89,90] These are contained in so-called large dense core vesicles (LDCVs), whereas small synaptic vesicles mostly store and release acetylcholine.[87,91,92] Catecholamine release and vesicles in

PC12 cells are further described in *Chapter 4.1.1 Vesicles, Neurotransmitters and Exocytosis*.

Commercially, two variants of PC12 cells are available: adherent and suspension cells. As they adhere poorly to non-coated substrates, suspension PC12 cells grow as aggregates floating in media. Conversely, adherent PC12 cells can be grown on a substrate (*e.g.*, culture dish or flask) coated with suitable materials (such as collagen or poly-D-lysine) to grow as a cell monolayer.[93] Although coating requires additional time and resources, adherence is advantageous for certain types of experiments, such as those requiring the cells to be immobile (*e.g.*, certain electrochemical techniques where an electrode is brought close to an individual cell), or resin embedded (so that they maintain their spatial organization and morphology). Therefore, the type of experimental protocol influences the choice between suspension and adherent cells.

PC12 cells are easy to culture and have been studied extensively, so that a lot of information is available regarding their proliferation and differentiation.[93] When grown with nerve growth factor, they differentiate into a phenotype which resembles sympathetic ganglion neurons, featuring neurite-like processes and varicosities.[87,94–96] Additionally, they are extremely versatile in terms of pharmacological manipulation; for example, vesicle volume and catecholamine accumulation can be modulated by incubating the cells with agents such as L-DOPA or reserpine,[97,98] and calcium homeostasis can be dysregulated *via* treatment with the peptide β-amyloid.[99]

Undifferentiated PC12 cells generally have a round morphology and can grow in clusters when cultured adherently; **Figure 9** shows some TEM images of adherent PC12 cells.

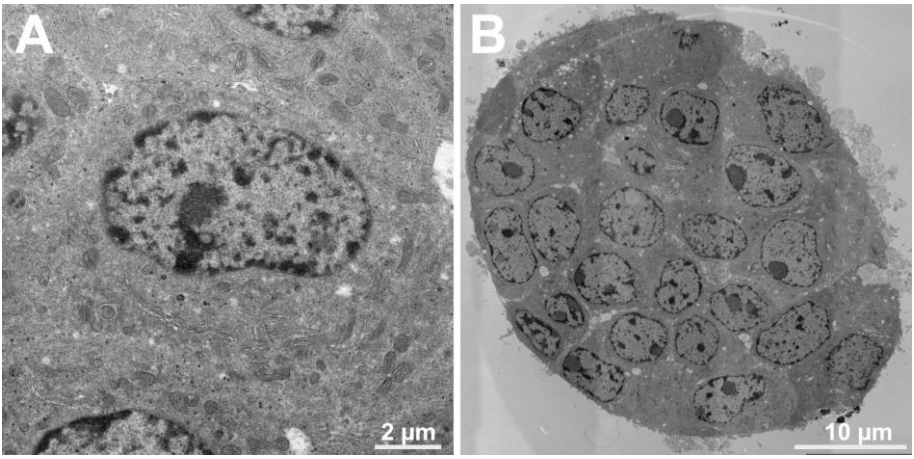

Figure 9. TEM images of adherent PC12 cells grown on poly-D-lysine coated glass-bottom dishes. (**A**) A PC12 cell. (**B**) Several stitched images acquired with a TEM tiling software (MAPS) showing several PC12 cells growing in a cluster. The cells were chemically fixed, resin embedded and thin sectioned prior to imaging.

2.3 Stem Cells and Neuronal Progenitor Cells (NPCs)

Embryonic stem cells (ESCs) were first isolated by two independent research groups in 1981.[100,101] ESCs are derived from blastocysts and have the ability to differentiate into any type of cell, so they are *totipotent*.[102] Induced pluripotent stem cells (iPSCs) were first reported by Takahashi and Yamanaka in 2006 in two liminal publications,[103,104] which described how adult mouse and human somatic cells could be converted into a pluripotent state (the ability to differentiate into cells from any germ layer) by using specific combinations of reprogramming factors, which are biologically active molecules that bind to cell receptors to affect the proliferation and differentiation fate of a cell by altering its gene expression.[105] Since ethical concerns surround the use of ESCs as they are derived from embryos, iPSCs have revolutionized the field of stem cell biology by offering an alternative source of stem cells, although some differences exist in cells derived from either type. Nevertheless, both ESCs and iPSCs exhibit high potency, making them extremely useful in regenerative medicine, drug discovery, and disease modeling.[82,102] Stem cells can be expensive and difficult to maintain, but their relevance in disease research cannot be overstated as they offer an invaluable tool for studying the mechanisms underlying diseases.

Neuronal progenitor cells. The central nervous system (CNS), comprising the brain and the spinal cord, is a vast network of cells that provides an organism with the ability to perceive and react to the environment.[106] The mammalian CNS is composed of two major types of cells, *i.e.*, neurons and glial cells. Neurons are specialized in intercellular communication and are therefore mainly involved in molecular signaling; they comprise a cell body, dendrites, and axons.[107] Glial cells (such as astrocytes and oligodendrocytes) play important roles in the development and functioning of the nervous system, especially in terms of neuronal survival and chemical environment; for example, oligodendrocytes form the myelin sheaths which protect some axons and enable quicker nerve signaling, and astrocytes help regulate neurotransmitter levels in the environment of the nervous system.[107,108]

In the CNS, NPCs are the precursor cells from which neurons and glial cells differentiate from; as they can grow into different cell types, they are pluripotent. Some images of NPCs are shown in **Figure 10**. NPCs have been shown to change their competency in differentiation during development, *i.e.*, their differentiation fate includes the sequential generation of different types of cells: in fact, their proliferation happens both symmetrically (one NPC dividing into two NPCs) and asymmetrically (one NPC dividing into various combinations of NPCs, basal progenitor cells, neurons and/or glial cells).[109] Therefore, they are vital in neurogenesis and the maturation and activity of the CNS.

NPCs are a heterogeneous group of cells with different differentiation potentials: depending on the specific factors used for differentiation, iPSCs can develop into distinct subtypes of NPCs, such as midbrain, forebrain, and hindbrain NPCs. Embryonic stem cells and iPSCs can be differentiated into NPCs *via* exposure to specific growth factors, which affect signaling pathways to mimic the natural development of the CNS. For example, SMAD (small worm phenotype, SMA, Mothers Against Decapentaplegic, MAD) proteins are involved in many cellular processes, including cell differentiation, and their inhibition has been shown to induce neuronal conversion in cultured iPSCs. Dual SMAD inhibition can greatly promote the differentiation of iPSCs into NPCs by modulation of signaling pathways which inhibit neuronal

differentiation.[110,111] The Wingless-related integration site (Wnt) pathway is also involved in the proliferation of midbrain and hindbrain cells and its activation can promote the differentiation of iPSCs into NPCs.[112] Finally, the Hedgehog pathway regulates the proliferation and survival of NPCs and can be activated by the Sonic Hedgehog protein, which affects differentiation fate in a concentration-dependent manner (*e.g.*, a low concentration differentiates the cells into midbrain NPCs, while a higher one differentiates the cells into forebrain NPCs).[111]

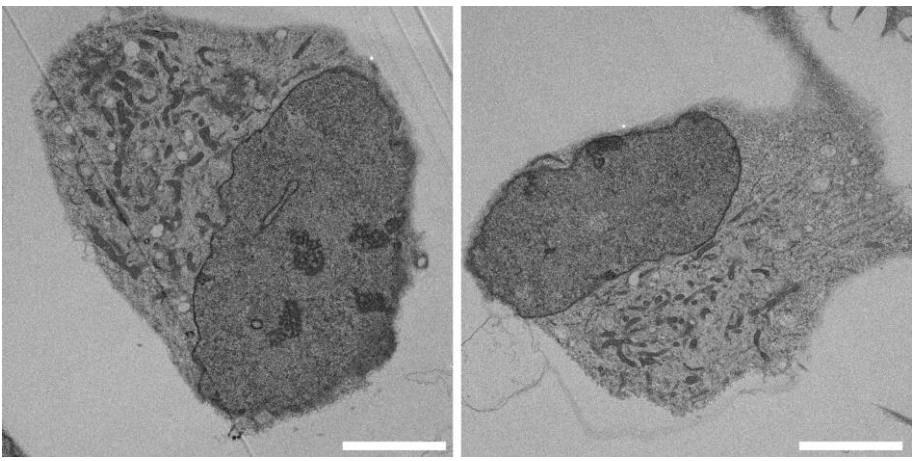

Figure 10. TEM images of NPCs grown on poly-D-lysine- and laminin coated glass bottom dishes. The cells were chemically fixed, resin embedded and thin sectioned prior to imaging. Scale bars are 5 μm.

Overall, the choice of biological sample type plays an important role in imaging studies, and cells are a versatile and widely available option. Cells can be prepared for imaging in a large variety of ways, which require careful optimization. Some are discussed in the next chapter.

CHAPTER 3. Sample Preparation

3.1 Principles of Biological Sample Preparation for Chemical Imaging

Overview. Sample preparation is a critical step in chemical imaging because any changes to the sample (*e.g.*, compositional changes, artifacts, damage) introduced during preparation will be reflected in the resulting images. Therefore, preserving structural fidelity and native chemical state of a sample is of outmost importance.[113] Biological samples can be prepared in a variety of ways, and the choice of preparation can depend on the type of instrument that is to be used for analysis; for example, some instruments operate under ultrahigh vacuum (UHV) conditions, which limits the type of preparation that is viable. For most analysis under a vacuum, samples need to be fixed and dehydrated; NanoSIMS operates under UHV, so any correlative approach using this technique requires sample fixation. Samples can be fixed in different ways, and some are outlined next. For TEM, samples often additionally use heavy metals (*e.g.*, osmium tetroxide, uranyl acetate) for contrast and these are applied before the sample is embedded in resin and sectioned; some details about these preparations are also discussed. Here, these are related to the topics of correlative imaging using electron microscopy (EM), fluorescence microscopy (FM) and NanoSIMS for the analysis of biological samples, specifically.

Fixing. Sample fixation minimizes degradation and stabilizes components. In chemical imaging, this is mostly aimed at maintaining the structure of a sample so that acquired images represent the original morphology and chemistry as closely as possible. Different techniques have been developed for the fixation of cell and tissue samples: the most common ones are chemical fixation and cryo-fixation.

Chemical fixation involves incubating a sample with a fixative, usually an aldehyde (namely formaldehyde and glutaraldehyde (GA)), to cross-link chemical components. This can be performed at room temperature

and does not require special equipment, so it is the most common fixation approach.

Formaldehyde penetrates rapidly into biological material owing to its small size, and mostly cross-links proteins and DNA bases by creating methylene bridges between N-terminal amino groups.[114] A mechanism of how formaldehyde links two proteins is shown in **Figure 11A**.[115] The reaction induced by formaldehyde is partially reversible, which limits its application.[116] Paraformaldehyde (PFA), a polymer of formaldehyde, cross-links more effectively and can reduce reversibility; PFA can also be mixed with GA (*e.g.*, as in Karnovsky fixative, which was first reported by Morris J. Karnovsky in 1965[117]) to further strengthen fixation. The first report of GA synthesis is credited to Harries and Tank in 1908.[118–120] After being commercialized in the 1950s and then introduced as a fixative in electron microscopy in the 1960s, its superior ability to preserve biological material compared to PFA quickly granted it a dominant role in preparation protocols.[119–121] GA is larger than PFA so it penetrates slower into specimens; therefore it is sometimes best suited for thin samples (*e.g.*, cell monolayers). A mixture of GA and PFA can be used for perfusion fixation or fixation of thick samples (*e.g.*, tissues).[122] GA is predominantly used to fix proteins by cross-linking functional groups (mainly amino) of the side chains of proteins, thus bridging neighbouring proteins.[65] It is present in solution as polymers of variable size; high-purity (*e.g.*, EM grade) GA comprises oligomers (mostly trimers) which ensures GA can efficiently penetrate the macromolecules of a biological sample. A mechanism of how GA links to proteins is shown in **Figure 11B**.[123] Usually, its reaction with proteins in thin samples, such as cell monolayers, is relatively fast, *i.e.*, minutes to hours, the time required for fixation being dependent on the properties of the sample (such as its thickness). A disadvantage of GA is that, at high concentrations, it may quench fluorescent proteins, and it is thus sometimes not suitable for FM studies, for which a gentler fixation with PFA might be preferred.[124,125] After fixation, free aldehyde groups need to be thoroughly washed off the sample with a buffer to avoid non-specific binding in the case of subsequent antibody labeling;[123] washing with a

primary amine (*e.g.*, glycine) can additionally ensure quenching of unreacted aldehyde residues.[122]

The buffers used for the different fixatives can vary; sodium cacodylate, 1,4-Piperazinediethanesulfonic acid (PIPES), 4-(2-hydroxyethyl)-1-piperazineethanesulfonic acid (HEPES) and phosphate-buffered saline (PBS) are some common ones. The choice of buffer can depend on the required characteristics (*e.g.*, pH, osmolality, compatibility with other reagents).[65,126] Osmotic effects (*e.g.*, cell shrinkage) can be minimized by selecting the right fixative solution (*e.g.*, fixative concentration, type of buffer) and protocol (*e.g.*, temperature, rate) for a specific sample.[65,122]

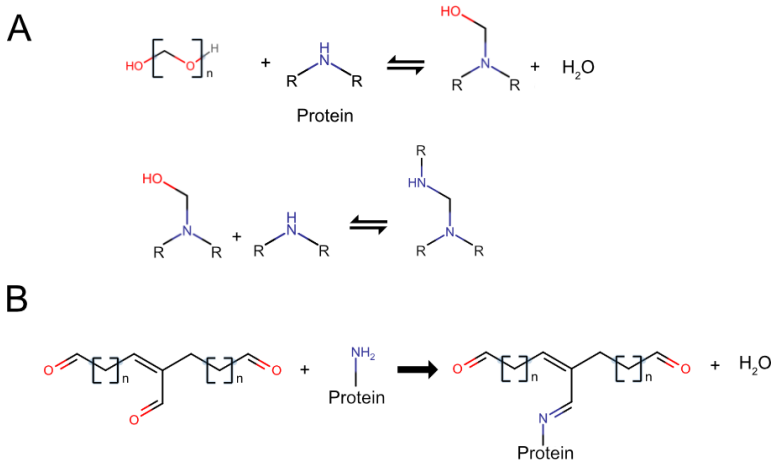

Figure 11. Proposed reaction mechanisms for primary protein fixation with formaldehyde (**A**) and GA (**B**).[115,123] Molecules were drawn at https://chem-space.com/search.

Cryo-fixation refers to fixation performed under cryogenic conditions. Cryo-fixation can help maintain a sample morphology more representative of the original state of the sample because it does not involve severe chemical reactions between a fixative and the sample constituents. The disadvantages of this approach include the need for specialized equipment, time-intensive procedures, skilled personnel, and overall financial costs. Freezing a sample might also limit the application of certain types of analysis, such as labeling approaches, the

use of cryo-sensitive specimens, or time-sensitive workflows. Furthermore, it might be entirely unsuitable for correlative imaging approaches where the correlated technique is not cryo-compatible. Therefore, cryo-fixation is not practical or feasible for some procedures. Nevertheless, it remains a useful technique for several applications, and one that provides invaluable insights into the capabilities of imaging at the cellular and molecular levels, especially in the EM field. Two of the main ways to cryo-fix small biological samples such as cells and small tissues are high-pressure freezing (HPF) and plunge freezing; larger samples, such as large pieces of tissue, may be better fixed using other techniques such as cold metal block freezing and jet freezing.[122,127]

HPF was reported in 1968 by Moor and Riehle,[128,129] and has since been established as an excellent way to preserve cellular ultrastructure. In HPF, high pressure (~2000 Bar) is applied to the sample in the range of 20 ms which generates a rapid drop of temperature down to -180 °C which is maintained by transferring the sample in liquid nitrogen.[122,130] This inhibits the formation of ice crystals and leads to the vitrification of the water molecules in the sample. The sample is then dehydrated in what is called *freeze-substitution*, a process by which the water in the sample is replaced with an organic solvent, commonly acetone, through ramping temperature (typically starting from -80 to -90 °C up to room temperature). Fixatives and contrasting agents can also be introduced during this step to enhance structural preservation and contrast, and the frozen state of the sample additionally minimizes fixation gradients because the fixative diffuses while the sample is already immobilized. After dehydration, the sample is typically embedded in resin.[122] Other approaches are also available, such as freeze-fracture, in which the high-pressure frozen sample is broken apart by applying a mechanical force and the resulting exposed fracture plane can be used for imaging.[131]

While relatively thick samples can be fixed using HPF, freezing is not as rapid as with other cryo-fixation techniques, which can be a disadvantage in certain applications.[113] Plunge freezing is faster than HPF but limited to thinner samples, such as cell monolayers. In plunge freezing, a sample is rapidly immersed into a cryogenic liquid, such as

propane or ethane, to be immobilized. Various parameters determine the efficiency of plunge freezing, such as plunge velocity, type of cryogen, sample size and substrate type.[122] Plunge frozen samples can be further freeze-substituted and resin embedded, or they can be directly followed by cryo-imaging such as with a cryo-TEM instrument. Finally, so-called *cryoprotectants* (*e.g.*, glycerol) can be introduced to a sample to reduce water content and further minimize formation of ice crystals, although this can affect the natural state of a biological environment, contradicting the fundamental purpose of cryo-fixation.[132]

Contrasting. The contrast of EM images can be enhanced by staining the samples with contrasting agents prior to imaging. Some of these agents, notably osmium tetroxide, uranyl acetate, and potassium permanganate, can additionally provide secondary fixation (*post-fixation*);[126] others, such as tannic acid, only act as stains.[133] The purpose of contrasting is to stain a biological component in order to generate a final image in which ultrastructures can better be discerned. Heavy metal contrasting can quench fluorescent proteins, which limits its applicability to Correlative Light and Electron Microscopy (CLEM) studies; this can sometimes be managed by lowering the concentration of the contrasting agent,[134,135] which generally requires compromising the EM image quality.

As it contains a heavy metal, osmium tetroxide has high electron density which causes beam scattering during EM imaging (see *Chapter 1.3.3 Transmission Electron Microscopy (TEM)*), therefore adding contrast to an image.[136] As a fixative, it acts by binding primarily to unsaturated fatty acids by reacting with the alkenes and forming cyclic esters; some of the proposed mechanisms are shown in **Figure 12**.[65,137] Therefore, using osmium tetroxide on cell samples results in strong lipid fixation, while also greatly enhancing cell membrane contrast during TEM imaging. Light emission from fluorescent proteins and dyes can be compromised in oxidizing conditions, and as it is a strong oxidizing agent, osmium tetroxide can quench fluorescence signals, even at low concentrations.[133,134] Uranyl acetate, another contrasting agent with a poorly understood reaction mechanism, similarly fixes proteins and lipids by binding to phosphate and amino groups, and also adds contrast

to EM images.[65,126] However, to generate the highest amount of contrast, it provides the best results when used in combination with osmium tetroxide.

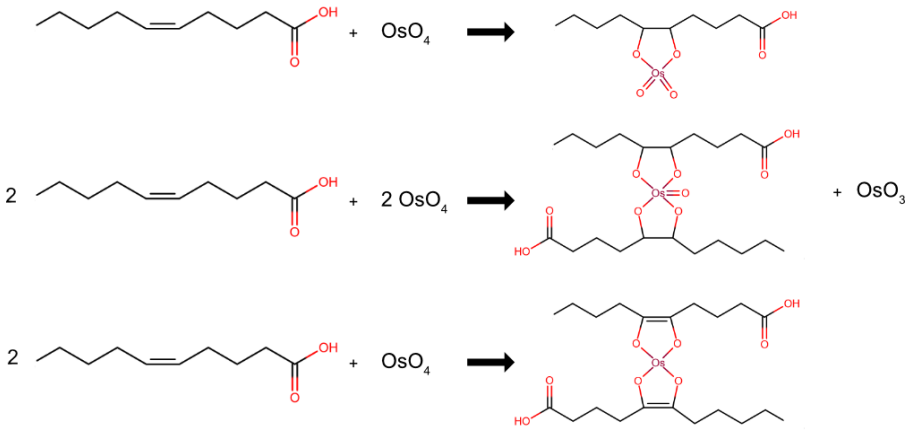

Figure 12. Proposed reaction mechanisms for secondary fixation with osmium tetroxide.[65,137] Molecules were drawn at https://chem-space.com/search.

Resin embedding. After fixation and contrasting, samples can be dehydrated (water is replaced with alcohol) and resin embedded. Different types of resins have different properties which must be considered when devising a preparation protocol. Resin infiltration involves replacing the liquid (such as the alcohol from dehydrated sample) with a polymer. Embedding and curing the infiltrated sample (*e.g.*, with heat or UV light) will result in a cross-linked, hardened block of resin which is easy to store, section and mount on a substrate for analysis.[65]

Resin infiltration of a dehydrated sample, commonly required in EM preparations, consists of a few steps. The first step is gradually replacing the alcohol in the sample with the resin. Since resin is typically more viscous than alcohol, gradient baths (of resin and alcohol, starting with the lowest resin ratio) are performed to allow the resin to penetrate the sample. The last bath, containing only resin, embeds the sample; gelatine or plastic capsules can provide a cast which is filled with resin. The resin is then polymerized, generally with heat (in an oven) or with UV light, yielding a block of variable hardness

depending on the type of resin used. A picture of resin blocks in gelatine casts is shown in **Figure 13A**. Shrinkage, texture and thermal stability can also differ between resins.[65] Two of the main categories of resins are epoxy and acrylic resins.

The representative unit of epoxy resin (or simply *epoxy*) is epoxide groups. Epoxy hardening agents create tight cross-linking to the epoxide groups, and the proportions of epoxy:hardener determines the extent of the cross-linking, and in turn, the hardness of the cured resin. Epoxy has the lowest shrinkage rate (<2%) of all resins and results in uniform, stable polymerization, and hard blocks which are easy to section. Araldite and Epon, two types of epoxy, are reportedly also very stable under a TEM electron beam, therefore they are a popular choice.[65] Nevertheless, the tight cross-linking and heat curing involved with some epoxies can cause structural changes such as protein denaturation, which can result in loss of antigenicity and reduce the ability of fluorescent probes or antibodies to bind to their targets.[126,136] Acrylic resins are less viscous than epoxy and can be cured at high (*e.g.*, LR White resin) or low (*e.g.*, Lowicryl resin) temperature. They generally have lower stability under an electron beam, and have a softer polymerization so they are more difficult to section; but, as some can be cured without heat, they have the advantage of being compatible with temperature-sensitive samples.[65,124,136,138]

Sectioning. Samples for TEM analysis must be sectioned into thin slices, typically ~70-300 nm in thickness, to be imaged. This is because the electron beam needs to pass through the section and arrive at the detector to create the final image. Therefore, sections must be cut from a resin block and placed onto a substrate suitable for analysis.

Sectioning can be performed with an ultramicrotome, which allows holding and cutting a block at a determined thickness with high precision. Fixed and embedded cell samples, whether as a pellet or monolayer, are contained in the resin block which is initially trimmed to expose the *face* (flat top) in a trapezoid shape. Some pictures of resin blocks after trimming are shown in **Figure 13B and C**. The trimmed block is then mounted on the microtome and the thin sections obtained with a specialized knife. Using a diamond knife ensures the highest

section quality (*e.g.*, uniform thickness, smoothness, integrity). The sections, which are very delicate, are then carefully placed on a substrate; for TEM, this is typically a copper grid, which can be coated with plastic (for example Formvar) for better support; glass coverslips, silica wafers and other substrates can be chosen for other types of analysis such as FM and SIMS. Cryo-sectioning is also available and allows a frozen sample to be cut at cryogenic conditions, so that it remains frozen throughout the process. Despite the advantages of cryo-analysis, the throughput of cryo-sectioning remains significantly lower and the process more cost-intensive.[124,136]

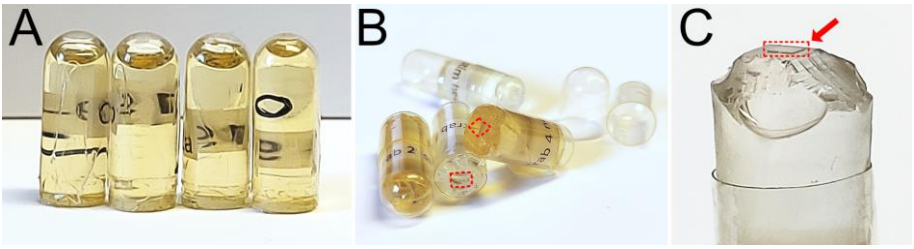

Figure 13. Agar 100 (yellow) and LR White (clear) resin blocks. (**A**) Resin blocks before trimming, stored in gelatine capsules. (**B**) Resin blocks after trimming, red dotted line outlines the trapezoid area. (**C**) Resin block after trimming, close-up of the trapezoid area (red dotted line and arrow).

3.2 Cell Sample Preparation for Correlative TEM/FM and NanoSIMS

Correlative TEM/NanoSIMS. To correlate TEM and NanoSIMS, samples need to be fixed because both techniques operate under UHV. Adherent cells can be fixed either as a monolayer or in a pellet; monolayers retain the spatial organization of a culture better than pellets, which involve resuspending cells that have been chemically or physically detached from the substrate they were growing on. Suspension cells are generally fixed as pellets.

While cryo-TEM is available, cryo-NanoSIMS has not yet been implemented commercially, meaning the NanoSIMS instrument currently only offers room-temperature analysis. Cell samples need to be either chemically fixed, high-pressure frozen and freeze-substituted,

or plunge frozen and freeze-substituted, to allow for room-temperature sectioning and imaging. Usually, the most practical approach is chemical fixation, which provides a good compromise between applicability and accessibility in many experimental settings. A generic schematic of TEM sample preparation steps is illustrated in **Figure 14**.

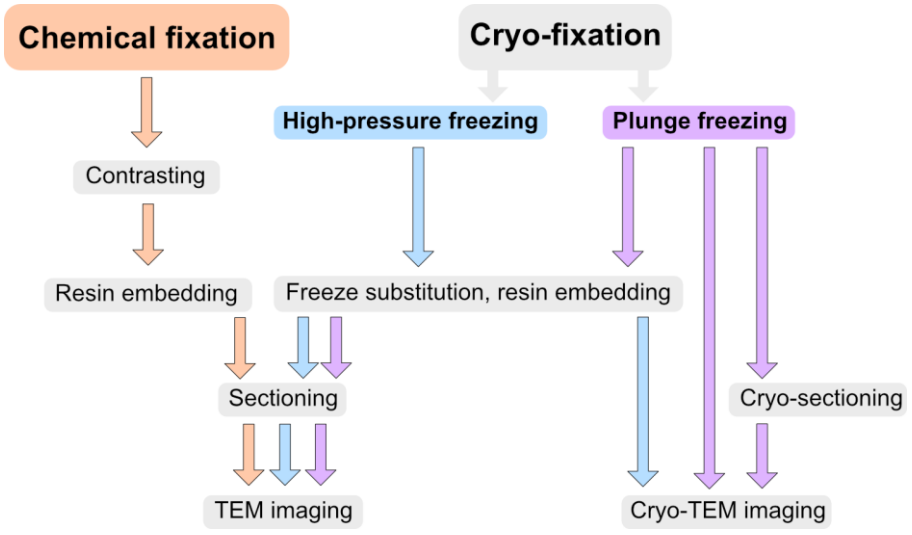

Figure 14. Schematics of room temperature TEM and cryo-TEM sample preparation steps.

Since TEM and NanoSIMS don't involve immunochemistry, cells can be embedded using epoxy resin. While holders for different types of substrates (grids, coverslips, silica wafers, and more) are available for the NanoSIMS, TEM holders are more limited, and generally require the use of specialized grids. Therefore, samples for correlative TEM and NanoSIMS should be placed on a substrate that is compatible with both instruments, such as EM copper grids. So-called *finder* grids can be used to facilitate the correlative imaging: they feature a grid pattern with reference points in the form of letters and numbers which offer a simple way to identify the exact position of a cell during both TEM and NanoSIMS imaging. This is because the reference points are visible not only on the TEM, but also on the NanoSIMS CCD camera, which is used to find the desired location for acquiring an image. A picture of a finder grid and how it is seen on the TEM and the NanoSIMS is shown in **Figure 15**.

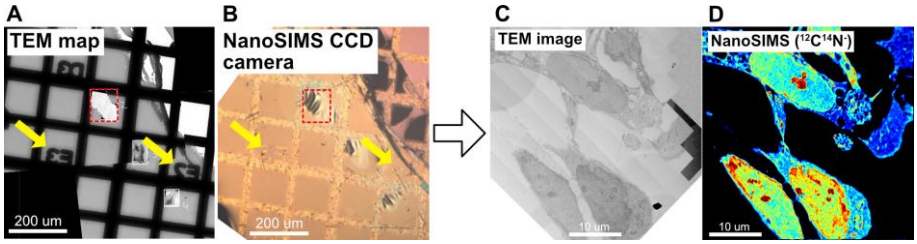

Figure 15. A finder grid as seen in the TEM (**A**) and NanoSIMS CCD camera (**B**). The same cell can be easily located owing to the reference letters and numbers (yellow arrows) on the grid and imaged with TEM (**C**) and NanoSIMS (**D**).

Correlative FM/NanoSIMS. While FM can be performed on live cell samples, samples for correlative FM and NanoSIMS must be fixed because the NanoSIMS is operated in UHV. Embedding usually requires the use of acrylic resins such as LR white, which does not quench fluorescence and does not auto fluoresce (other resins, such as Epon, can have high autofluorescence which may hinder FM).[10] Fixed, embedded and sectioned samples are placed onto a substrate compatible with the different types of imaging and instrument holders. As finder grids are not ideal for FM, locating the same cells with both techniques is contingent on the type of substrate used; for example, after imaging a cell on a section on a silica wafer with FM, locating the same cell on the NanoSIMS requires finding its location based on fiducials such as section edges and halos conferred by the shape of the cells. Despite being challenging, this is sufficiently practical for both techniques. **Figure 16** shows an example of how cells on sections of silica wafers are imaged with FM and can then be precisely located on the NanoSIMS.

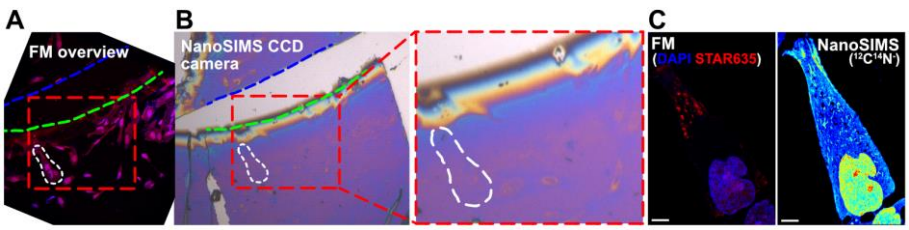

Figure 16. Location of single cells on a section of a silica wafer in the NanoSIMS CCD camera. A large field of view image of an area is taken with the FM (**A**) and brightness/contrast adjusted so that reference points (*e.g.*, section edges and blemishes; some examples with the blue and green lines) are visible and can be used to locate the area of interest (red box) on the NanoSIMS

CCD camera (**B**). By doing so, single cells can be accurately located and imaged with both techniques. (**C**) A target cell imaged with FM and NanoSIMS. Scale bars are 10 µm.

In summary, the choice of sample preparation protocol can have a significant impact on the quality of the analysis and results and should therefore be carefully considered. Fixation, contrasting, embedding, and sectioning choices should be tailored to the specific type of sample and analytical parameters. By optimizing protocols, it is possible to address a variety of scientific questions in the most efficient and effective way. In the next chapter, some of the scientific questions that can be examined with the different sample preparation methods to carry out correlative NanoSIMS and EM/FM are discussed.

CHAPTER 4. Research Topics for the Application of Correlative NanoSIMS and EM/LM

4.1 Intercellular Communication

4.1.1 Vesicles, Neurotransmitters and Exocytosis

Cellular communication *via* secretion is a vital activity which begins with the genesis, packaging, and release of transmitter molecules to the outside of the cell. In a cell, so-called *synaptic vesicles* (sometimes called *granules*) are packaged with molecular cargo, such as elemental ions (*e.g.*, H^+, Ca^{2+}, Mg^{2+}), adenosine triphosphate (ATP), proteins, and neurotransmitters.[139] After packaging, a vesicle travels to the plasma membrane, docks and fuses with it, and releases part or all of its contents. This liberates the vesicle cargo in the extracellular space, to be promptly picked up by other cells *via* receptors. This is known as *exocytosis*, a complex process by which cells can communicate with each other through the release and exchange of molecular transmitters. Some components and mechanisms of exocytosis are discussed next.

Synaptic vesicles and exocytosis. As neurotransmitter carriers, vesicles play a central part in exocytosis. Vesicles are small (typically ~50-350 nm diameter), membrane-bound spherical organelles which bud from the Golgi apparatus. Their membrane is composed of a phospholipid bilayer decorated with a variety of membrane-associated proteins, which are a crucial machinery involved in exocytosis. These include soluble *N*-ethylmaleimide-sensitive factor attachment protein receptor (SNARE) proteins, synaptotagmin1, Rab proteins, and Sec1/Munc18-like (SM) proteins.[140–142]

SNAREs are a family of proteins which are collectively found both on the vesicle and the target (plasma) membrane; they include synaptobrevin, syntaxin1 and Synaptosome Associated Protein 25 (SNAP25). Synaptobrevin (also known as vesicle-associated membrane protein, VAMP) is associated with the vesicle membrane, while syntaxin1 and SNAP25 are associated with the plasma membrane.[141]

Most SNARE proteins share a common SNARE *motif*, a characteristic amino acid sequence composed of 60-70 residues,[143,144] and they are thought to be pivotal in mediating the fusion of the vesicle with the target membrane (cleavage of SNAREs has been shown to inhibit neurotransmission).[145,146] During the initial stage of vesicle fusion, known as *priming*, the SNARE motifs assemble into a complex (the so-called *SNARE complex*) which facilitates the fusion (*zippering*) of the two negatively charged lipid bilayers at the membranes junction, which is otherwise hindered by an activation energy barrier.[144,147] The concerted action of SM proteins is thought to facilitate zippering.[143] After priming, vesicle fusion is triggered by a rapid influx of Ca^{2+} ions through the plasma membrane. This influx is suggested to be catalyzed by the Ca^{2+}-binding protein synaptotagmin1,[148–150] which is thought to additionally promote the SNARE complex formation and zippering.[151,152] The fusing of the vesicle and plasma membrane finally generates a *fusion pore*, an opening through which the vesicle contents are released to the extracellular space. A schematic of the exocytosis process is illustrated in **Figure 17A**. After the formation of the pore, the vesicle can either entirely collapse and release its contents fully (this is known as *all-or-none*, or *full* release), or only release a fraction of its contents and subsequently close again. Two mechanisms of fractional release are known, namely *kiss-and-run* and *partial* release. In kiss-and-run, the fusion pore is very small (~2 nm in diameter),[153,154] and releases only a small fraction of the vesicle contents; whereas in partial release, a bigger fraction escapes by the opening of a larger fusion pore.[154–161] A schematic of the three release modes is presented in **Figure 17B**. Since the different modalities of exocytosis can be altered in different ways, and elicit different cell responses, the determination of the dynamics of release are an important research topic.

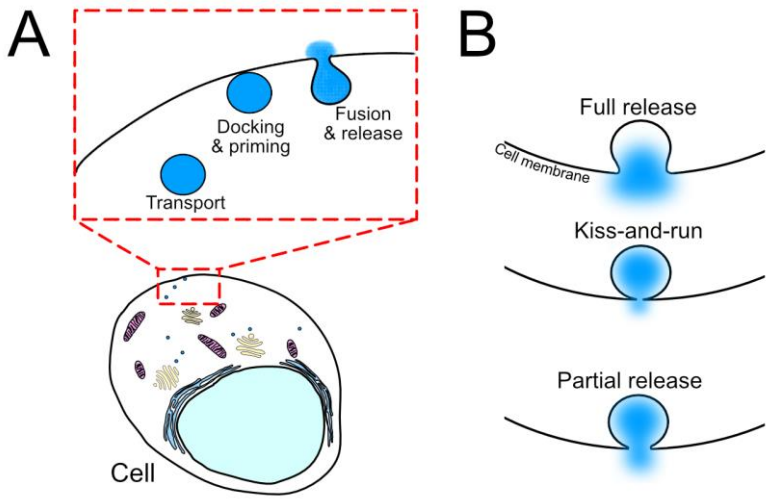

Figure 17. Simplified schematics of some exocytosis mechanics. (**A**) Illustration of a cell with vesicles translocating to the plasma membrane, docking and priming, and releasing the vesicular content to the extracellular space. (**B**) Illustration of the three known modes of exocytosis release (full release, kiss-and-run, partial release). Vesicle content is colored in blue.

Dopamine. Neurotransmitters can be of several kinds and be categorized in different ways. Some of these include acetylcholine, amino acids (*e.g.*, gamma-aminobutyric acid, glycine, glutamate, aspartate), amines (for example catecholamines, indolamines), peptides (*e.g.*, endorphins) and purines (for example ATP and adenosine).[107] Catecholamines are a category of amine neurotransmitter which includes dopamine, norepinephrine and epinephrine. In PC12 cells, the main neurotransmitter contained in vesicles is dopamine. Dopamine is loaded into the vesicles *via* a vesicular monoamine transporter, VMAT2, a protein present on the vesicle membrane (VMAT1 is a similar transporter which is found in vesicles of chromaffin cells of adrenal medulla);[162] following exocytosis, dopamine is picked up by another cell *via* receptors of the G-protein coupled receptors family, namely the D1 and D2 receptors and their subfamilies.[163,164] The chemical precursor of dopamine is L-3,4-dihydroxyphenylalanine (L-DOPA), which is synthesized into dopamine in the cell *via* dopa-decarboxylase.[165] In the human brain, dopamine is involved in many important functions such as locomotion, positive reinforcement, and cognition;[166] it is produced in the ventral tegmental area, which releases

it to the nucleus accumbens and prefrontal cortex, and the substantia nigra, which release it to the striatum, primarily. It is additionally produced by the hypothalamus and released in the pituitary gland, inhibiting production of the hormone prolactin.[107,167]

Large dense core vesicles (LDCVs). Secretory vesicles in PC12 cells are of two types: small synaptic vesicles and large dense core vesicles (LDCVs).[40] Synaptic vesicles are small (typically up to 50 nm in diameter) while LDCVs are larger (typically up to 350 nm in diameter); other than size, the latter distinguish themselves by presenting with a core which is dense with proteins (hence their name).[87] This core is often clearly visible in electron microscopy images of PC12 cells: as mentioned earlier, a denser region in the sample appears darker compared to a background in a TEM image, which makes the dense core easily discernible from the lucent part of a LDCV (the so-called *halo*). Examples of this are shown in **Figure 18**. The proteins comprising the dense core matrix are mainly chromogranins, of which chromogranin A (CgA) is quantitatively the most abundant. Modulation of CgA content in LDCVs has been shown to affect both neurotransmitter storage and exocytosis, which highlights the pivotal role of dense core proteins in vesicle dynamics.[168] The halo, which surrounds the dense core, mostly contains ions (such as Ca^{2+} and H^{+}), ATP, and a portion of neurotransmitters, and it maintains an intravesicular pH of ~5.5.[139] Since vesicles keep a stable neurotransmitter concentration, osmotic equilibrium is also maintained by resizing of the halo.[98] The dense core acts as a reservoir for neurotransmitters, such as catecholamines, which bind to the core matrix due to electrostatic forces (*e.g.*, attractive forces between the negatively charged amino acid residues in the proteins of the dense core, and the catecholamines, which are protonated under the acidic conditions of the vesicle).[169] By tightly binding neurotransmitter molecules, the dense core facilitates the packaging of very high levels of neurotransmitter within vesicles.[170] The separation between dense core and halo, as well as the different neurotransmitter content of these intravesicular compartments, has been measured with analytical techniques such as electrochemistry and MSI.[40,169,171,172]

Overall, understanding the structure and properties of vesicles can provide insights into the exocytosis process, and inform the understanding of how cells communicate and how exocytosis can be modulated.

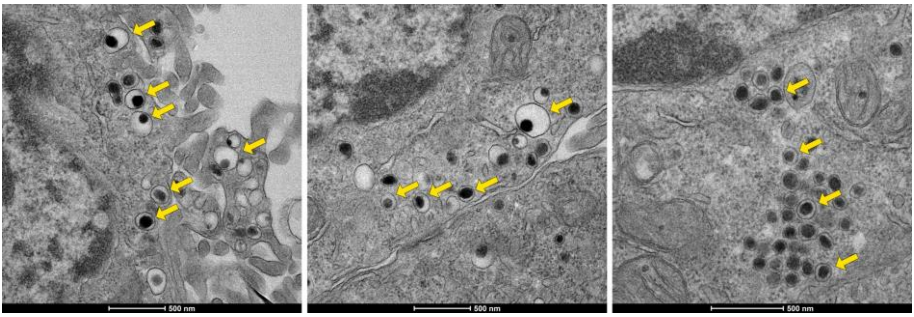

Figure 18. Transmission electron microscopy images of large dense core vesicles (LDCVs) in PC12 cells. The yellow arrows point to some examples of LDCVs, where dense core (dark region) and halo (light region) are clearly discernible.

4.1.2 Application of Correlative Imaging for the Study of Cellular Communication

Correlative electron and light microscopy (CLEM). Chemical imaging of cells can provide valuable information into the mechanisms underlying intercellular communication. Understanding complex biochemical processes is facilitated by multimodal imaging approaches which provide a more detailed sample characterization compared to single-technique approaches.

Electron microscopy (EM) provides the ultrastructure of a cell with high lateral resolution. Yet, since cellular communication involves processes which are highly dynamic, EM alone can be limited in the quality of information that it provides. CLEM combines the strengths of EM and light microscopy (often FM) and has seen growing applications in recent years. CLEM was introduced in the 1970s and promptly showcased its potential by confirming the identity of cellular structures which had been elusive with unimodal microscopy.[173] One of the first CLEM publications demonstrated the value of combining several microscopic techniques: time-lapse cinematography, immunofluorescence, and scanning and transmission electron

microscopy were performed sequentially on interacting macrophages and tumor cells to study macrophage-mediated cytotoxicity. Morphological information of individual cells was obtained with either FM or EM separately,[174] *i.e.*, the "correlation" was meant as the application of different techniques to characterize a sample, rather than directly analysing the same sample with different imaging modalities.[175] CLEM was finally applied the same sample in the 1980s with studies on macrophages and white blood cells.[176,177] Since then, several cellular communication processes have been studied with CLEM, including endocytosis, membrane trafficking, cell-cell interactions, and cell signaling.[178–180]

CLEM can leverage the broad field of view of a light microscope to localize rare, fluorescently labeled events (*e.g.*, transfection efficiency) and can be used to provide information about the location of a fluorescent protein within the ultrastructural architecture of a cell.[124,175] One of the main challenges of CLEM is preserving the integrity of the sample throughout the preparation protocol, which is sometimes incompatible (*e.g.*, resin embedding for EM can cause denaturation and partial quenching of fluorescent proteins).[173] Cryo-CLEM is an effective approach which allows observation of a sample in its native state without the need for resin embedding, but one that requires inconvenient and costly sample handling.[124] For this reason, CLEM workflows often involve FM imaging on live samples prior to fixation and embedding, necessary for EM, which limits the applicability of the technique. One of the first reports of CLEM on pre-fixed samples illustrated the possibility to use a hydrophilic resin which does not quench fluorescence significantly.[181] There are other aspects of EM sample preparation that can impede CLEM, such as heavy metal staining, which can also quench fluoerscence.[133,182] The so-called *resolution gap*, *i.e.*, the difference in lateral resolution between EM and FM, can also be a challenge when correlating images, and this has been addressed by the development of super-resolution FM techniques such as photoactivated localization microscopy (PALM), stochastic optical reconstruction microscopy (STORM), and STED; in fact, the first report of PALM was in correlation with TEM.[183]

Correlative EM/FM and NanoSIMS. EM and SIMS are well-suited for correlation because they require similar sample preparation. For example, they both involve UHV analysis, such that samples need to be dehydrated and fixed before imaging. The trade-off is that this precludes the possibility to perform live-imaging.

Nevertheless, the strengths and capabilities of EM and NanoSIMS provide a powerful combination for the investigation of cellular communication components such as secretory vesicles. Vesicles are nanoscale organelles which are discernible in TEM images, but in a NanoSIMS image alone they cannot be distinguished. Therefore, to definitively localize vesicles in a NanoSIMS image, correlation with TEM is necessary.

Figure 19 illustrates a TEM and NanoSIMS correlative workflow which allows vesicles and other organelles in the SIMS image to be localised, and consequently obtain their chemical information (*e.g.*, isotopic enrichment). Cells are grown as a monolayer on a glass-bottom dish, incubated with an isotopically labeled molecule, chemically fixed, embedded in resin, and thin sectioned. A cell is then imaged with both TEM and NanoSIMS, revealing the localization of the incorporated isotope into the compartments of the cell. Following similar protocols, TEM and NanoSIMS have been used in studies on vesicles and exocytosis and investigated aspects such as exocytotic release modes (*e.g.*, partial release), dynamics of vesicular dopamine loading, and localization of dopamine in subvesicular compartments.[40,155,172]

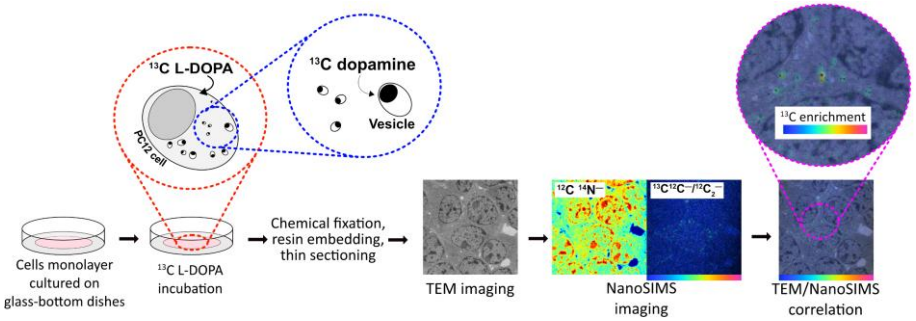

Figure 19. Schematic of a sample preparation and correlative imaging workflow for the localization of an isotopic label in single cells. Cells are cultured on a glass-bottom dish, incubated with ^{13}C L-DOPA, which is transported into the cell, converted into ^{13}C dopamine

and loaded into vesicles. TEM and NanoSIMS imaging provide the ultrastructure (TEM) and chemical composition (NanoSIMS) of the cell, and the $^{13}C^{12}C/^{12}C_2$ NanoSIMS ratio image localizes the isotopic enrichment within the cell.

FM and NanoSIMS have also been correlated to investigate aspects of cellular communication, such as cell signaling and metabolic exchange.[184–186] For example, by using NanoSIMS and STED imaging, the protein turnover at individual synapses of neuronal cells was found to correlate with synapse activity, giving insights into the connection between these two processes.[187] NanoSIMS and fluorescence *in situ* hybridization (FISH) have also been extensively used correlatively, as these methods can provide complementary information, for example, on the metabolic activities of microbial populations.[188]

4.2 Cellular Stress, Stress Granules and Protein Turnover

4.2.1 Cellular Stress, RNP Granules and Mechanisms of Stress Granules

Cellular stress can be defined as any event inflicting a strain on the physiological homeostasis of the system. The cellular homeostasis response compensates for strains *via* adjustment mechanisms, aimed at restoring equilibrium. If the strain is too severe, the cellular stress response (CSR) is activated with the aim of repairing and stabilizing macromolecules as well as restoring cell-cycle checkpoints. Failure to restore the homeostatic state eventually leads to a breaking point which prompts system collapse (*e.g.*, apoptosis).[189,190]

The cellular stress response. Stress can impair the normal protein turnover of cells. Protein turnover refers to the continuous cycle of synthesis and degradation of proteins and is an essential mechanism for adequate cellular function. Impairment of protein turnover due to accumulation of unfolded or misfolded proteins, denaturation, or formation of protein aggregates, and insufficient or abnormal post-translational modifications, can cascade a system to collapse.

There are many ways in which cells can be stressed. For example, heat shock can cause aberrant protein conformations which ultimately impair protein function.[191] The heat shock response is one of the main CSR mechanisms. It was first observed in 1962 in the fruit fly,[192] and

its name originates from its early descriptions of a response to hyperthermia;[193] it is now known that other than being only caused by heat, the heat shock response can be activated by many other types of stressors, including oxidative stress and heavy metal exposure. Proteins are damaged as a consequence of exposure to excess heat. The heat shock response increases the expression of chaperones which refold the affected proteins, with the aim of minimizing protein loss of functionality and toxicity.[194]

The unfolded protein response, which was initially discovered in glucose-deprived yeast,[195] consists of signaling pathways activated by three sensors, namely inositol-requiring enzyme 1 (IRE1), activating transcription factor 6 (ATF6) and protein kinase RNA-like endoplasmic reticulum kinase (PERK). Jointly, these sensors are aimed at reactivating ER function *via* the unleash of specialized chaperones and restoration of proper protein conformations.[195,196] The unfolded protein response is a response to endoplasmic reticulum (ER) stress, which can arise, for example, from glucose starvation, oxygen deprivation, and calcium dysregulation. These can impair and inhibit the protein folding ability of the ER and lead to accumulation of misfolded proteins.[197] Other perturbations in cellular homeostasis can additionally propagate to the ER and indirectly trigger the unfolded protein response.[197] In addition, ER stress and unfolded protein response inefficiency have been implicated in diseases such as neurodegenerative diseases (NDs), cancer, and metabolic disorders.[198]

RNA-binding proteins and stress granules. RNA-binding proteins (RBPs) are important components in the CSR, as they contribute to the formation of so-called *stress granules* (SGs). SGs are non-membrane-bound organelles which can form in the event of cellular stress; they are a type of ribonucleoprotein (RNP) granule, other types including nuclear bodies, P-bodies, storage granules, and transport granules.[199] SGs are protein-messenger RNA (mRNA) assemblies with the theorized function of protecting and/or triaging non-translating mRNA during stress;[200–202] while the response of mRNA metabolism to stress and SG formation has been linked to cellular pathophysiology,[203–205] the definite function and dynamics of SGs are an ongoing topic of debate and research.

SGs comprise many different RNPs which can be classified according to their characteristics. For example, some RNPs can promote SG formation when overexpressed. These include Ras-GTPase-activating SH3-domain-binding protein 1 (G3BP1), T-cell intracellular antigen-1 (TIA-1), and cell cycle associated protein (CAPRIN). In addition, SG formation can be inhibited when these proteins are knocked down/out.[206–208] Other RNPs have been described as entirely dispensable for SG assembly, *i.e.*, SGs can still form when the protein is downregulated.[206] SG-associated RNPs have also been observed to compartmentalize between substructures, *i.e.*, inner cores and surface.[209,210] This implies that some RNPs are rigidly located within the SGs, while surface RNPs dynamically translocate in and out of them. This distinction is made according to the RNA affinity of an RNP, whereby the exchange rate of the protein represents the off-rate from RNA.[211] RNPs which are highly dynamic in SGs, create SGs when overexpressed, and reduce SG formation when downregulated, have been termed *kinetic condensers*. An interesting role of kinetic condensers is that of facilitating or even allowing SG formation, and for this reason such proteins can be considered hallmarks of SGs.[206] G3BP1 falls into this category, and it has been shown that increasing the RNA-binding capacity of G3BP1 reduces its mobility in SGs, further suggesting that a lower off-rate results in a less dynamic behaviour.[212] Furthermore, it has been suggested that SGs sequester specific mRNA species, *i.e.*, mRNA with different transcripts are redistributed during stress between cytoplasm and SGs,[213] and that translation of mRNA sequestered into SGs resumes after stress recovery.[210]

Current models suggest that SGs aggregate in cells *via* liquid-liquid phase separation (LLPS) promoted by weak dynamic interactions between SG-associated proteins and mRNA. LLPS occurs when a heterogeneous liquid separates into distinct liquid compartments (*phases*) due to the differing chemical properties and intermolecular forces of their constituents. Since the interactions among SG components are multivalent (*e.g.*, binding rates can vary significantly), they have been described as both liquid- and solid-phase assemblies; the cores being more solid-like, and the surface being more liquid-like.[209] This implies that stable interactions between their proteins are present in the SG cores, possibly favored by a higher concentration of proteins and tighter mRNA binding.[209,214]

Stress granules in neurodegenerative disease. Protein aggregates have been connected to several NDs, such as Alzheimer´s disease and amyotrophic lateral sclerosis (ALS),[215,216] and vast amounts of literature exist which probe the complexities of these diseases. Proteins from protein aggregates in NDs are mainly degraded by two systems: the ubiquitin-proteasome system and the phagosome-lysosome system.[217] The activity of the ubiquitin-proteasome system plays an important regulatory role in protein metabolism, and SGs have been implicated in the functioning of this highly complex mechanism; for example, the ubiquitin-proteasome system has been shown to be negatively affected in cells which are SG-deficient, further indicating that SG are essential in the sequestration of misfolded cytosolic proteins in some biological models.[218]

In the event of chronic cellular stress (*e.g.*, NDs), SGs can become persistent structures.[219] ALS is a common ND characterized by the progressive degeneration of motor neurons and consequent dysfunction of muscles.[220,221] While the direct causes of ALS are unknown, it has been linked to cellular abnormalities such as mitochondrial dysfunction, aberrant protein aggregation, and defective RNA metabolism.[219] Many RNA-binding proteins are known to cause ALS when mutated.[222] For example, mutations in the genes encoding TAR DNA-binding protein 43 (TDP-43) and fused in sarcoma (FUS) have both been identified in ALS cases,[223,224] and accumulation of TDP-43 has been shown to be associated with SGs.[225] In fact, TDP-43 has been linked to SG dynamics *via* regulation of SG proteins such as G3BP1 and TIA-1.[226] Alzheimer´s disease, a ND which commonly presents with memory loss, behavioral changes, and cognitive impairment, has been linked to dysregulation of the protein-degradation pathways. Genetic variants or altered expression levels of degradation regulators have been reported in Alzheimer´s disease human brain tissues and Alzheimer´s disease mouse models.[227–231] The mechanisms underlying these NDs are complex and revealing their neurobiological intricacies requires thorough and comprehensive analysis.

Overall, SGs can be described as dynamic organelles with complex structures and functions. Detailing SG mechanisms can elucidate their role in pathophysiology and may lead to further understanding of how cells respond to diseases associated with SG dysfunction. Since SG

dysfunction is implicated in the aberrant pathological protein aggregates that occur in many NDs, further studies into SG dynamics such as assembly, persistence, disassembly, and degradation are warranted.

4.2.1 Application of Correlative Imaging for the Study of Cellular Stress

Correlative FM and NanoSIMS. While several studies on SGs have utilized microscopy techniques, typically FM,[232–234] correlative imaging of SGs and their components is not as common. FM of SGs involves the tagging of SG-associated proteins with fluorescent proteins which can be imaged with a fluorescence microscope, thereby identifying and localizing target proteins sequestered in SGs. Although some studies have used EM to image SGs in cells,[235] antibody labeling is still necessary to accurately locate them. SGs are also not recognizable in a NanoSIMS image so correlation with FM is again necessary.

By incubating cells with an isotopic amino acid, correlative FM and NanoSIMS imaging becomes possible and allows one to obtain, for example, localization and structural information about SGs in cells as well as information about their protein incorporation and turnover. **Figure 20** shows an example of a STED/NanoSIMS correlative workflow for the study of SGs and cellular stress. Cells are grown as a monolayer on a glass-bottom dish, they are incubated with an isotopically labeled (*e.g.*, ^{15}N) amino acid, which is incorporated in the cell into proteins. The cells are then stressed (*e.g.*, chemically) and fixed. SGs are labeled with a fluorescent protein and the samples are resin embedded and thin sectioned. STED imaging is performed and localizes the SGs in the cells; NanoSIMS is then performed, and isotope uptake is measured within the cells. Precise overlaying of the same cells imaged with both techniques is feasible and supplies a broader characterization of the sample compared to unimodal imaging.

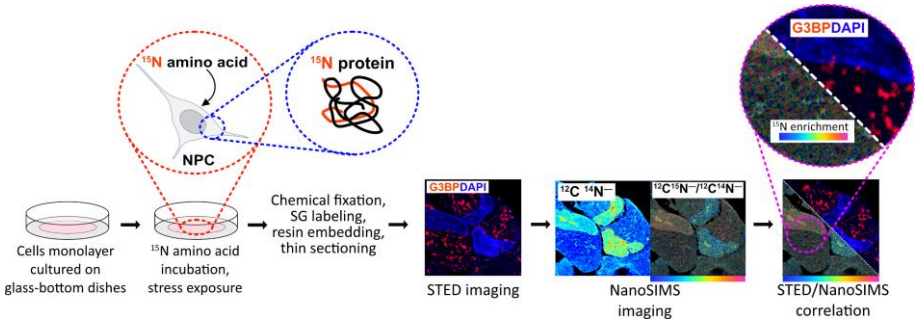

Figure 20. Schematic of a sample preparation and correlative imaging workflow for the localization of an isotopic label and SGs in single cells. Cells are cultured on a glass-bottom dish, incubated with a ^{15}N amino acid, which is transported into the cell and metabolized into ^{15}N proteins. STED and NanoSIMS imaging provide the localization and chemical composition of the SGs, respectively, and the $^{12}C^{15}N/^{12}C^{14}N$ NanoSIMS ratio image measures the isotopic enrichment within the individual SGs, as well as in the entire cell.

NanoSIMS is a powerful and versatile instrument. Despite its limitations, which can be overcome to some extent by correlating the technique with other imaging modalities such as TEM and FM, it can provide invaluable data. In fact, a variety of research questions, including cellular communication and cellular stress, can benefit from being explored using a correlative approach. To conclude, correlative chemical imaging offers a flexible strategy to study fundamental processes of biological systems, which can shed light on the underlying mechanisms of cellular function and disease.

CHAPTER 5. Summary of Papers

5.1 Paper I

In **paper I**, NanoSIMS and transmission electron microscopy (TEM) were correlated to visualize large dense core vesicles (LDCVs) of PC12 cells which had been incubated with ^{13}C L-3,4-dihydroxyphenylalanine (L-DOPA). The isotopically labeled L-DOPA was uptaken by the cells and synthesized into dopamine, and finally loaded into LDCVs *via* membrane transporters. TEM allowed imaging of the ultrastructure of the cells and vesicles, and NanoSIMS allowed the localization of the isotope label corresponding to the newly loaded dopamine. The lateral resolution capabilities of NanoSIMS were pushed to discern the intravesicular compartments of LDCVs enabling the distinction between their dense core and halo. Labeled dopamine was localized and quantified in each compartment separately and appeared as being preferentially stored in the dense core. Additionally, absolute quantification of local dopamine concentration was accomplished.

5.2 Paper II

In **paper II**, NanoSIMS was correlated with stimulated emission-depletion (STED) microscopy to image stress granules (SGs) in neuronal progenitor cells (NPCs) which had been incubated with an isotopically labeled amino acid and stressed with the endoplasmic reticulum (ER) stressor thapsigargin (TG). The correlation of STED and NanoSIMS facilitated the localization of individual SGs and the evaluation of their protein turnover at different stress-recovery time points. Additionally, cytoplasmic protein turnover of healthy *versus* stressed cells was studied and found to be severely impaired by ongoing ER stress.

5.3 Paper III

In **paper III**, NanoSIMS and TEM were correlated to investigate the role of vesicle size in the dynamics of partial release exocytosis events. PC12 cells were transfected with a dense core protein to modulate

LDCV size changes (discernible *via* TEM) and incubated with ^{13}C L-DOPA to localize isotopic dopamine uptake *via* NanoSIMS. It was found that different transfection methods affect vesicle size, and that fraction of release in partial release events does not correlate with vesicle size under the sample conditions implemented.

5.4 Paper IV

In **paper IV**, NanoSIMS and TEM were correlated to investigate the subcellular distribution of protein turnover in NPCs. NPCs were incubated with an isotopically labeled amino acids and organelle type was assessed using TEM. Protein turnover could be determined in different organelles and protein/amino acid half-lives could be calculated. Differences were found not only in the spatial distribution and incorporation of different amino acids but also between organelles, pointing to a heterogeneity of protein turnover within the cell.

CHAPTER 6. Concluding Remarks and Future Outlook

The focus of the work included in this thesis has been to apply correlative chemical imaging to analyze cell samples with a range of aims and objectives. Methods for the implementation of correlative imaging have been described, and in particular, the effective correlation between NanoSIMS, electron, and fluorescence microscopy to achieve thorough sample characterization. The work demonstrates the importance of selecting the best techniques, biological samples, and sample preparations, in order to answer selected scientific questions; this includes considerations into technical limitations, desired output, experimental costs, and time constraints.

The boundaries of correlative imaging can be explored and pushed by creating new protocols and workflows or by optimizing existing ones. Correlating different imaging methods requires knowledge of the strengths and limitations of each individual technique and of the best means to harness and combine them to achieve results in the most efficient and reasonable way. New technologies are continually being developed and this paves the way for new correlative approaches. For example, improvement of the NanoSIMS instrument to include cryo capabilities would open the door to correlative cryo-EM and cryo-NanoSIMS, allowing exploitation of the advantages of cryo sample preparation. Furthermore, the synthesis of new probes detectable by both fluorescence microscopy and NanoSIMS (*e.g.*, a fluorophore containing an isotopic tag or an element exogenous in cells) would enable easier image correlation and to spatially localize targets with even higher accuracy.

Overall, correlative chemical imaging is a powerful integrative tool offering versatile approaches for identifying and characterizing chemical and molecular components in biological systems such as single cells, and thus it can provide information about the composition and structure of cellular components, as well as data on the dynamics of cellular mechanisms.

Acknowledgments

First and foremost, I would like to acknowledge my main supervisor Prof. **Andrew Ewing**. Thank you for believing in me and giving me this opportunity to learn and improve myself. The personal and professional growth I went through during these years has been vastly beyond anything I could ever have imagined. I am forever grateful for this precious experience. I would like to equally acknowledge my second supervisor Asst. Prof. **Nhu Phan**, thank you for being an amazing teacher and mentor, I am truly grateful for everything I have learned from you during this time. To my third supervisor Dr. **Michael Kurczy**, thank you for engaging in all our discussions with so much enthusiasm and passion, and for everything you have taught me, it was immensely appreciated. I would also like to thank my examiner Prof. **Marica Ericson** for supporting and guiding me throughout my studies.

To **Alicia Lork** and **Tho Nguyen**, I could spend a lot of words saying how much I have enjoyed working and sharing this time with you, but it would never be enough. Thank you for being the best office partners and colleagues. To **Emmanuel Berlin**, thank you for being so patient with me and for always lending a hand (and an ear!), I am grateful and feel so lucky for our time together and everything I have learned from you. To Dr. **Chaoyi Gu**, **Kim Long** and Dr. **Andre Du Toit**, I have greatly enjoyed working with you, thank you for your passion and insights in our work together. To Dr. **Massimo Micaroni**, thank you for your genuine commitment and mentoring about all-things TEM and sample preparation. To Dr. **Aurélien Thomen** and Dr. **Elias Ranjbari**, thank you for your insights and for being so passionate in sharing your knowledge about NanoSIMS.

To **everyone working in the Andy Ewing Group and the Nhu Phan Group**, both currently and previously, you all taught me something valuable at some point and I am very grateful for having been a part of these amazing groups. Thank you for all the great discussions and our fun times together!!!

To Dr. **Michela Borghesan**, I am so grateful for the unconditional love and support. It made all the difference many times. Thank you for being a great friend and an even greater scientist. To **Mohammad Sadia**, thank you for believing in me, and for always helping without judgement. To **Cristina Otero Garcia**, I cannot be thankful enough for all the laughs and support during these years, they helped me get through the hardest moments. To **Francesca Zappa**, thank you for being there when I needed it the very most. Special thanks to **Lucian Mihai Obreja** and **Anna Albano**, without whom none of this would have been possible.

Further thanks to Massimo, Andre, Chaoyi, Emmanuel and Alicia for additional feedback and ideas during the writing of this thesis.

Finally, I would like to acknowledge the Centre for Cellular Imaging at the University of Gothenburg and the National Microscopy Infrastructure, NMI (VR-RFI 2016-00968) for providing assistance in electron microscopy, and the Chemical Imaging Infrastructure at the University of Gothenburg and Chalmers University of Technology, located at the Astra Zeneca BioVenture Hub, for the support with the NanoSIMS work.

References

(1) Terzioglu, R.; Aydin, G.; Soylu Koc, N.; Terzioglu, C. Investigation of the Structural, Magnetic and Electrical Properties of the Au Doped YBCO Superconductors. *J. Mater. Sci. Mater. Electron.* **2019**, *30*, 2265–2277.

(2) Xing, Y.; Xu, M.; Gui, X.; Cao, Y.; Babel, B.; Rudolph, M.; Weber, S.; Kappl, M.; Butt, H. J. The Application of Atomic Force Microscopy in Mineral Flotation. *Adv. Colloid Interface Sci.* **2018**, *256*, 373–392.

(3) Rudin, M.; Weissleder, R. Molecular Imaging in Drug Discovery and Development. *Nat. Rev. Drug Discov.* **2003**, *2*, 123–131.

(4) Willmann, J. K.; van Bruggen, N.; Dinkelborg, L. M.; Gambhir, S. S. Molecular Imaging in Drug Development. *Nat. Rev. Drug Discov.* **2008**, *7*, 591–607.

(5) da Cunha, M. M. L.; Trepout, S.; Messaoudi, C.; Wu, T. Di; Ortega, R.; Guerquin-Kern, J. L.; Marco, S. Overview of Chemical Imaging Methods to Address Biological Questions. *Micron*, 2016, *84*, 23–36.

(6) Magistretti, P. J.; Allaman, I. A Cellular Perspective on Brain Energy Metabolism and Functional Imaging. *Neuron* **2015**, *86*, 883–901.

(7) Hirsch, G. V; Bauer, C. M.; Merabet, L. B. Using Structural and Functional Brain Imaging to Uncover How the Brain Adapts to Blindness. *Ann. Neurosci. Psychol.* **2015**, *2*.

(8) Kherlopian, A. R.; Song, T.; Duan, Q.; Neimark, M. A.; Po, M. J.; Gohagan, J. K.; Laine, A. F. A Review of Imaging Techniques for Systems Biology. *BMC Syst. Biol.* **2008**, *2*, 1–18.

(9) Schmidt, R.; Fitzek, H.; Nachtnebel, M.; Mayrhofer, C.; Schroettner, H.; Zankel, A. The Combination of Electron Microscopy, Raman Microscopy and Energy Dispersive X-Ray Spectroscopy for the Investigation of Polymeric Materials. *Macromol. Symp.* **2019**, *384*, 1800237.

(10) Saka, S. K.; Vogts, A.; Kröhnert, K.; Hillion, F.; Rizzoli, S. O.; Wessels, J. T. Correlated Optical and Isotopic Nanoscopy. *Nat. Commun.* **2014**, *5*, 3664.

(11) McLoughlin, N.; Wacey, D.; Kruber, C.; Kilburn, M. R.; Thorseth, I. H.; Pedersen, R. B. A Combined TEM and NanoSIMS Study of Endolithic Microfossils in Altered Seafloor Basalt. *Chem. Geol.* **2011**, *289*, 154–162.

(12) Thomson, J. J. XL. Cathode Rays . *London, Edinburgh, Dublin Philos. Mag. J. Sci.* **1897**, *44*, 293–316.

(13) Van Der Heide, P. *Secondary Ion Mass Spectrometry: An Introduction to Principles and Practices*; John Wiley & Sons, 2014.

(14) Hoffmann, E. de; Vincent, S. *Mass Spectrometry: Principles and*

Applications; John Wiley & Sons, 2007.

(15) Mamyrin, B. A. Time-of-Flight Mass Spectrometry (Concepts, Achievements, and Prospects). *Int. J. Mass Spectrom.* **2001**, *206*, 251–266.

(16) Shampo, M. A.; Kyle, R. A.; Steensma, D. P. Frederick Soddy—Pioneer in Radioactivity. In *Mayo Clinic Proceedings*; Elsevier Ltd, 2011; Vol. 86, p. e39.

(17) Münzenberg, G. Development of Mass Spectrometers from Thomson and Aston to Present. *Int. J. Mass Spectrom.* **2013**, *349–350*, 9–18.

(18) Woodcock, K. S. The Emission of Negative Ions under the Bombardment of Positive Ions. *Phys. Rev.* **1931**, *38*, 1696–1703.

(19) Thompson, J. S. A New Method of Producing Negative Ions. *Phys. Rev.* **1931**, *38*, 1389.

(20) Arnot, F. L. A.; Milligan, J. C. M. A New Process of Negative Ion Formation. *Proc. R. Soc. London. Ser. A - Math. Phys. Sci.* **1936**, *156*, 538–560.

(21) Cameron, A. E.; Eggers Jr, D. F. An Ion "Velocitron." *Rev. Sci. Instrum.* **1948**, *19*, 605.

(22) McLafferty, F. W. Mass Spectrometry in Chemical Research and Production. *Appl. Spectrosc.* **1957**, *11*, 148–156.

(23) Gohlke, R. S. Time-of-Flight Mass Spectrometry and Gas-Liquid Partition Chromatography. *Anal. Chem.* **1959**, *31*, 535–541.

(24) Castaing, R.; Slodzian, G. Optique Corpusculaire-Premiers Essais de Microanalyse Par Emission Ionique Secondaire. *Comptes Rendus Hebd. Des Seances L Acad. Des Sci.* **1962**, *255*.

(25) Honig, R. E.; Woolston, J. R. Laser-induced Emission of Electrons, Ions, and Neutral Atoms from Solid Surfaces. *Appl. Phys. Lett.* **1963**, *2*, 138–139.

(26) Fenner, N. C.; Daly, N. R. Laser Used for Mass Analysis. *Rev. Sci. Instrum.* **1966**, *37*, 1068–1070.

(27) Spengler, B.; Hubert, M.; Kaufmann, R. MALDI Ion Imaging and Biological Ion Imaging with a New Scanning UV-Laser Microprobe. In *Proceedings of the 42nd Annual Conference on Mass Spectrometry and Allied Topics*; 1994; Vol. 1041, p. 1041.

(28) Caprioli, R. M.; Farmer, T. B.; Gile, J. Molecular Imaging of Biological Samples: Localization of Peptides and Proteins Using MALDI-TOF MS. *Anal. Chem.* **1997**, *69*, 4751–4760.

(29) Kompauer, M.; Heiles, S.; Spengler, B. Atmospheric Pressure MALDI Mass Spectrometry Imaging of Tissues and Cells at 1.4-Mm Lateral Resolution. *Nat. Methods* **2017**, *14*, 90–96.

(30) Zavalin, A.; Todd, E. M.; Rawhouser, P. D.; Yang, J.; Norris, J. L.; Caprioli, R. M. Direct Imaging of Single Cells and Tissue at Sub-Cellular Spatial Resolution Using Transmission Geometry MALDI

MS. *J. Mass Spectrom.* **2012**, *47*, 1473–1481.
(31) Takáts, Z.; Wiseman, J. M.; Gologan, B.; Cooks, R. G. Mass Spectrometry Sampling under Ambient Conditions with Desorption Electrospray Ionization. *Science.* **2004**, *306*, 471–473.
(32) Laskin, J.; Heath, B. S.; Roach, P. J.; Cazares, L.; Semmes, O. J. Tissue Imaging Using Nanospray Desorption Electrospray Ionization Mass Spectrometry. *Anal. Chem.* **2012**, *84*, 141–148.
(33) Swales, J. G.; Strittmatter, N.; Tucker, J. W.; Clench, M. R.; Webborn, P. J. H.; Goodwin, R. J. A. Spatial Quantitation of Drugs in Tissues Using Liquid Extraction Surface Analysis Mass Spectrometry Imaging. *Sci. Rep.* **2016**, *6*, 1–9.
(34) Kertesz, V.; Van Berkel, G. J. Liquid Microjunction Surface Sampling Coupled with High-Pressure Liquid Chromatography-Electrospray Ionization-Mass Spectrometry for Analysis of Drugs and Metabolites in Whole-Body Thin Tissue Sections. *Anal. Chem.* **2010**, *82*, 5917–5921.
(35) Rao, W.; Celiz, A. D.; Scurr, D. J.; Alexander, M. R.; Barrett, D. A. Ambient DESI and LESA-MS Analysis of Proteins Adsorbed to a Biomaterial Surface Using In-Situ Surface Tryptic Digestion. *J. Am. Soc. Mass Spectrom.* **2013**, *24*, 1927–1936.
(36) Müller, A.; Benninghoven, A. Investigation of Surface Reactions by the Static Method of Secondary Ion Mass Spectrometry. III. The Oxidation of Vanadium, Niobium and Tantalum in the Monolayer Range. *Surf. Sci.* **1973**, *39*, 427–436.
(37) Benninghoven, A.; Wiedmann, L. Investigation of Surface Reactions by the Static Method of Secondary Ion Mass Spectrometry. IV. The Oxidation of Magnesium, Strontium, and Barium in the Monolayer Range. *Surf. Sci.* **1974**, *41*, 483–492.
(38) Müller, A.; Benninghoven, A. Investigation of Surface Reactions by the Static Method of Secondary Ion Mass Spectrometry. V. The Oxidation of Titanium, Nickel, and Copper in the Monolayer Range. *Surf. Sci.* **1974**, *41*, 493–503.
(39) Benninghoven, A.; Müller, A. Investigation of Surface Reactions by the Static Method of Secondary Ion Mass Spectrometry. II. The Oxidation of Chromium in the Monolayer Range. *Surf. Sci.* **1973**, *39*, 416–426.
(40) Rabasco, S.; Nguyen, T. D. K.; Gu, C.; Kurczy, M. E.; Phan, N. T. N.; Ewing, A. G. Localization and Absolute Quantification of Dopamine in Discrete Intravesicular Compartments Using NanoSIMS Imaging. *Int. J. Mol. Sci.* **2021**, *23*, 160.
(41) Hoppe, P.; Cohen, S.; Meibom, A. NanoSIMS: Technical Aspects and Applications in Cosmochemistry and Biological Geochemistry. *Geostand. Geoanalytical Res.* **2013**, *37*, 111–154.

(42) IUPAC. Compendium of Chemical Terminology, 2nd Ed. (the "Gold Book"). Compiled by A. D. McNaught and A. Wilkinson. Blackwell Scientific Publications, Oxford (1997). XML on-line corrected version: http://goldbook.iupac.org (2006-) created by M. Nic, J. Jirat, B. Kosata; updates compiled by A. Jenkins. ISBN 0-9678550-9-8. doi:10.1351/goldbook.

(43) Murray, K. K. Resolution and Resolving Power in Mass Spectrometry. *J. Am. Soc. Mass Spectrom.* **2022**, *33*, 2342–2347.

(44) Mattauch, J.; Herzog, R. Über Einen Neuen Massenspektrographen. *Zeitschrift für Phys.* **1934**, *89*, 786–795.

(45) Kilburn, M. R.; Wacey, D. *Nanoscale Secondary Ion Mass Spectrometry (NanoSIMS) as an Analytical Tool in the Geosciences*; Royal Society of Chemistry, 2014.

(46) Vickerman, J. C.; Gilmore, I. S. *Surface Analysis: The Principal Techniques*; Vickerman, J. C.; Gilmore, I. S., Eds.; John Wiley & Sons, Ltd: Chichester, UK, 2009.

(47) Eckstein, W. Oscillations of Sputtering Yield. *Nucl. Instruments Methods Phys. Res. Sect. B Beam Interact. with Mater. Atoms* **2000**, *171*, 435–442.

(48) Wimmer, E.; Freeman, A. J.; Weinert, M.; Krakauer, H.; Hiskes, J. R.; Karo, A. M. Cesiation of W(001): Work Function Lowering by Multiple Dipole Formation. *Phys. Rev. Lett.* **1982**, *48*, 1128–1131.

(49) Gnaser, H. Exponential Scaling of Sputtered Negative-Ion Yields with Transient Work-Function Changes on-Bombarded Surfaces. *Phys. Rev. B - Condens. Matter Mater. Phys.* **1996**, *54*, 16456–16459.

(50) Tompa, G. S.; Carr, W. E.; Seidl, M. Work Function Reduction of a Tungsten Surface Due to Cesium Ion Bombardment. *Appl. Phys. Lett.* **1986**, *49*, 1511–1513.

(51) Van der Heide, P. A. W.; Azzarello, F. V. Work Function, Valence Band and Secondary Ion Intensity Variations Noted during the Initial Stages of SIMS Depth Profiling of Si and SiO2 by Cs+. *Surf. Sci.* **2003**, *531*, L369–L377.

(52) Thomen, A.; Najafinobar, N.; Penen, F.; Kay, E.; Upadhyay, P. P.; Li, X.; Phan, N. T. N.; Malmberg, P.; Klarqvist, M.; Andersson, S.; et al. Subcellular Mass Spectrometry Imaging and Absolute Quantitative Analysis across Organelles. *ACS Nano* **2020**, *14*, 4316–4325.

(53) Craig, H. Isotopic Standards for Carbon and Oxygen and Correction Factors for Mass-Spectrometric Analysis of Carbon Dioxide. *Geochim. Cosmochim. Acta* **1957**, *12*, 133–149.

(54) Fitzsimons, I. C. W.; Harte, B.; Clark, R. M. SIMS Stable Isotope Measurement: Counting Statistics and Analytical Precision. *Mineral. Mag.* **2000**, *64*, 59–83.

(55) Ogliore, R.; Nagashima, K.; Huss, G.; Haenecour, P. A Reassessment

of the Quasi-Simultaneous Arrival Effect in Secondary Ion Mass Spectrometry. *Elsevier* **2021**, *491*, 17–28.

(56) Ruska, E. The Development of the Electron Microscope and of Electron Microscopy. *Rev. Mod. Phys.* **1987**, *59*, 627–638.

(57) Egerton, R. F. *Physical Principles of Electron Microscopy: An Introduction to TEM, SEM, and AEM, Second Edition*; Springer, 2016.

(58) Darrigol, O. *A History of Optics: From Greek Antiquity to the Nineteenth Century*; Oxford University Press, 2012.

(59) Tbakhi, A.; Amr, S. S. Ibn Al-Haytham: Father of Modern Optics. *Ann. Saudi Med.* **2007**, *27*, 464–467.

(60) Binnig, G.; Rohrer, H. Scanning Tunneling Microscopy from Birth to Adolescence. *Rev. Mod. Phys.* **1987**, *59*, 615–625.

(61) Poggi, M. A.; Gadsby, E. D.; Bottomley, L. A.; King, W. P.; Oroudjev, E.; Hansma, H. Scanning Probe Microscopy. *Anal. Chem.* **2004**, *76*, 3429–3444.

(62) Williams, D. B.; Carter, C. B. The Transmisasion Electron Microscope. In *Transmission Electron Microscopy*; Springer US, 1996; pp. 3–17.

(63) Penczek, P. A. Resolution Measures in Molecular Electron Microscopy. In *Methods in Enzymology*; Academic Press Inc., 2010; Vol. 482, pp. 73–100.

(64) Baker, L. A.; Smith, E. A.; Bueler, S. A.; Rubinstein, J. L. The Resolution Dependence of Optimal Exposures in Liquid Nitrogen Temperature Electron Cryomicroscopy of Catalase Crystals. *J. Struct. Biol.* **2010**, *169*, 431–437.

(65) Ayache, J.; Beaunier, L.; Boumendil, J.; Ehret, G.; Laub, D. *Sample Preparation Handbook for Transmission Electron Microscopy: Techniques*; Springer Science & Business Media, 2010.

(66) Srot, V.; Watanabe, M.; Scheu, C.; Van Aken, P. A.; Salzberger, U.; Luerßen, B.; Janek, J.; Rühle, M. Characterization of Chemical Composition and Electronic Structure of Pt/YSZ Interfaces by Analytical Transmission Electron Microscopy. *Solid State Ionics* **2010**, *181*, 1616–1622.

(67) Ponce, A.; Mejía-Rosales, S.; José-Yacamán, M. Scanning Transmission Electron Microscopy Methods for the Analysis of Nanoparticles. In *Nanoparticles in Biology and Medicine: Methods and Protocols*; Methods Mol Biol, 2012; Vol. 906, pp. 453–471.

(68) Ulloa-Navas, M. J.; Pérez-Borredá, P.; Morales-Gallel, R.; Saurí-Tamarit, A.; García-Tárraga, P.; Gutiérrez-Martín, A. J.; Herranz-Pérez, V.; García-Verdugo, J. M. Ultrastructural Characterization of Human Oligodendrocytes and Their Progenitor Cells by Pre-Embedding Immunogold. *Front. Neuroanat.* **2021**, *15*.

(69) Sanderson, M. J.; Smith, I.; Parker, I.; Bootman, M. D. Fluorescence

Microscopy. *Cold Spring Harb. Protoc.* **2014**, *2014*, 1042–1065.
(70) Hell, S. W.; Wichmann, J. Breaking the Diffraction Resolution Limit by Stimulated Emission: Stimulated-Emission-Depletion Fluorescence Microscopy. *Opt. Lett.* **1994**, *19*, 780.
(71) Vicidomini, G.; Bianchini, P.; Nature, Diaspro -, A. STED Super-Resolved Microscopy. *Nature* **2018**, *15*, 173–182.
(72) Suzuki, T.; Matsuzaki, T.; Hagiwara, H.; Aoki, T.; Takata, K. Recent Advances in Fluorescent Labeling Techniques for Fluorescence Microscopy. *Acta Histochem. Cytochem.* **2007**, *40*, 131–137.
(73) Shimomura, O.; Johnson, F. H.; Saiga, Y. Extraction, Purification and Properties of Aequorin, a Bioluminescent Protein from the Luminous Hydromedusan, Aequorea. *J. Cell. Comp. Physiol.* **1962**, *59*, 223–239.
(74) Liu, S. L.; Wang, Z. G.; Xie, H. Y.; Liu, A. A.; Lamb, D. C.; Pang, D. W. Single-Virus Tracking: From Imaging Methodologies to Virological Applications. *Chem. Rev.* **2020**, *120*, 1936–1979.
(75) Davis, L. *Basic Methods in Molecular Biology*; Elsevier, 2012.
(76) Washington, I. M.; Van Hoosier, G. Clinical Biochemistry and Hematology. In *The Laboratory Rabbit, Guinea Pig, Hamster, and Other Rodents*; Elsevier, 2012; pp. 57–116.
(77) Chawla, R. *Practical Clinical Biochemistry: Methods and Interpretations - Ranjna Chawla - Google Böcker*; JP Medical Ltd., 2014.
(78) Wang, D.; Bodovitz, S. Single Cell Analysis: The New Frontier in "Omics." *Trends Biotechnol.* **2010**, *28*, 281–290.
(79) Shay, J. W.; Wright, W. E. Hayflick, His Limit, and Cellular Ageing. *Nature* **2000**, *1*, 72–76.
(80) Hayflick, L.; Moorhead, P. S. The Serial Cultivation of Human Diploid Cell Strains. *Exp. Cell Res.* **1961**, *25*, 585–621.
(81) Hayflick, L. The Limited in Vitro Lifetime of Human Diploid Cell Strains. *Exp. Cell Res.* **1965**, *37*, 614–636.
(82) Eglen, R.; Reisine, T. Primary Cells and Stem Cells in Drug Discovery: Emerging Tools for High-Throughput Screening. *Assay Drug Dev. Technol.* **2011**, *9*, 108–124.
(83) Jedrzejczak-Silicka, M. History of Cell Culture. In *New Insights into Cell Culture Technology*; 2017; pp. 1–29.
(84) Lucey, B. P.; Nelson-Rees, W. A.; Hutchins, G. M. Henrietta Lacks, HeLa Cells, and Cell Culture Contamination. *Arch. Pathol. Lab. Med.* **2009**, *133*, 1463–1467.
(85) Stacey, G. *Primary Cell Cultures and Immortal Cell Lines*; Wiley, 2005.
(86) Irfan Maqsood, M.; Matin, M. M.; Bahrami, A. R.; Ghasroldasht, M. M. Immortality of Cell Lines: Challenges and Advantages of Establishment. *Cell Biol. Int.* **2013**, *37*, 1038–1045.

(87) Greene, L. A.; Tischler, A. S. Establishment of a Noradrenergic Clonal Line of Rat Adrenal Pheochromocytoma Cells Which Respond to Nerve Growth Factor. *Proc. Natl. Acad. Sci.* **1976**, *73*, 2424–2428.
(88) Lam, A. K. yin. Update on Adrenal Tumours in 2017 World Health Organization (WHO) of Endocrine Tumours. *Endocr. Pathol.* **2017**, *28*, 213–227.
(89) Westerink, R. H. S.; Ewing, A. G. The PC12 Cell as Model for Neurosecretion. *Acta Physiol.* **2007**, *192*, 273–285.
(90) Greene, L. A.; Rein, G. Release, Storage and Uptake of Catecholamines by a Clonal Cell Line of Nerve Growth Factor (NGF) Responsive Pheochromocytoma Cells. *Brain Res.* **1977**, *129*, 247–263.
(91) Schubert, D.; LaCorbiere, M.; Klier, F. G.; Steinbach, J. H. The Modulation of Neurotransmitter Synthesis by Steroid Hormones and Insulin. *Brain Res.* **1980**, *190*, 67–79.
(92) Travis, E. R.; Wightman, R. M. Spatio-Temporal Resolution of Exocytosis from Individual Cells. *Annu. Rev. Biophys. Biomol. Struct.* **1998**, *27*, 77–103.
(93) Wiatrak, B.; Kubis-Kubiak, A.; Piwowar, A.; Barg, E. PC12 Cell Line: Cell Types, Coating of Culture Vessels, Differentiation and Other Culture Conditions. *Cells* **2020**, *9*.
(94) de los Rios, C.; Cano-Abad, M. F.; Villarroya, M.; López, M. G. Chromaffin Cells as a Model to Evaluate Mechanisms of Cell Death and Neuroprotective Compounds. *Pflugers Arch. - Eur. J. Physiol.* **2018**, *470*, 187–198.
(95) Matsuzaki, Y.; Maruta, R.; Takaki, K.; Kotani, E.; Kato, Y.; Yoshimura, R.; Endo, Y.; Whitty, C.; Pernstich, C.; Gandhi, R.; et al. Sustained Neurotrophin Release from Protein Nanoparticles Mediated by Matrix Metalloproteinases Induces the Alignment and Differentiation of Nerve Cells. *Biomolecules* **2019**, *9*, 510.
(96) Mingorance-Le Meur, A.; Mohebiany, A. N.; O'Connor, T. P. Varicones and Growth Cones: Two Neurite Terminals in PC12 Cells. *PLoS One* **2009**, *4*, e4334.
(97) Sombers, L. A. The Effects of Vesicular Volume on Secretion through the Fusion Pore in Exocytotic Release from PC12 Cells. *J. Neurosci.* **2004**, *24*, 303–309.
(98) Colliver, T. L.; Pyott, S. J.; Achalabun, M.; Ewing, A. G. VMAT-Mediated Changes in Quantal Size and Vesicular Volume. *J. Neurosci.* **2000**, *20*, 5276–5282.
(99) Zhou, Y.; Gopalakrishnan, V.; Richardson, J. S. Actions of Neurotoxic β-Amyloid on Calcium Homeostasis and Viability of PC12 Cells Are Blocked by Antioxidants but Not by Calcium Channel Antagonists. *J. Neurochem.* **1996**, *67*, 1419–1425.
(100) Martin, G. R. Isolation of a Pluripotent Cell Line from Early Mouse

Embryos Cultured in Medium Conditioned by Teratocarcinoma Stem Cells. *Proc. Natl. Acad. Sci. U. S. A.* **1981**, *78*, 7634–7638.
(101) Evans, M.; Nature, M. K.-; 1981, U. Establishment in Culture of Pluripotential Cells from Mouse Embryos. *Nature* **1981**, *292*, 154–6.
(102) Robinton, D. A.; Daley, G. Q. The Promise of Induced Pluripotent Stem Cells in Research and Therapy. *Nature* **2012**, *481*, 295–305.
(103) Takahashi, K.; Yamanaka, S. Induction of Pluripotent Stem Cells from Mouse Embryonic and Adult Fibroblast Cultures by Defined Factors. *Cell* **2006**, *126*, 663–676.
(104) Takahashi, K.; Tanabe, K.; Ohnuki, M.; Narita, M.; Ichisaka, T.; Tomoda, K.; Yamanaka, S. Induction of Pluripotent Stem Cells from Adult Human Fibroblasts by Defined Factors. *Cell* **2007**, *131*, 861–872.
(105) Stone, W. L.; Leavitt, L.; Varacallo, M. *Physiology, Growth Factor*; StatPearls Publishing, 2017.
(106) Ludwig, P. E.; Varacallo, M. *Neuroanatomy, Central Nervous System (CNS)*; StatPearls Publishing, 2017.
(107) *Neuroscience: Third Edition*; Purves, D.; Augustine, G. J.; Fitzpatrick, D.; Hall, W. H.; LaMantia, A.-S.; McNamara, J. O.; Williams, S. M., Eds.; 3rd ed.; Sinauer Associates, Inc., 2003.
(108) Jessen, K. R. Glial Cells. *Int. J. Biochem. Cell Biol.* **2004**, *36*, 1861–1867.
(109) Kageyama, R.; Ohtsuka, T.; Shimojo, H.; Imayoshi, I. Dynamic Regulation of Notch Signaling in Neural Progenitor Cells. *Current Opinion in Cell Biology*, 2009, *21*, 733–740.
(110) Chambers, S. M.; Fasano, C. A.; Papapetrou, E. P.; Tomishima, M.; Sadelain, M.; Studer, L. Highly Efficient Neural Conversion of Human ES and IPS Cells by Dual Inhibition of SMAD Signaling. *Nat. Biotechnol.* **2009**, *27*, 275–280.
(111) Jefri, M.; Bell, S.; Peng, H.; Hettige, N.; Maussion, G.; Soubannier, V.; Wu, H.; Silveira, H.; Theroux, J. F.; Moquin, L.; et al. Stimulation of L-Type Calcium Channels Increases Tyrosine Hydroxylase and Dopamine in Ventral Midbrain Cells Induced from Somatic Cells. *Stem Cells Transl. Med.* **2020**, *9*, 697–712.
(112) Kandel, E. R.; Schwartz, J. H.; Jessell, T. M.; Siegelbaum, S.; Hudspeth, A.J. and Mack, S. *Principles of Neural Science, Vol. 4*; New York: McGraw-hill, 2000.
(113) McDonald, K. Cryopreparation Methods for Electron Microscopy of Selected Model Systems. *Methods Cell Biol.* **2007**, *79*, 23–56.
(114) Hoffman, E. A.; Frey, B. L.; Smith, L. M.; Auble, D. T. Formaldehyde Crosslinking: A Tool for the Study of Chromatin Complexes. *J. Biol. Chem.* **2015**, *290*, 26404–26411.
(115) Darvell, B. W. *Materials Science for Dentistry - 10th Edition*;

Woodhead publishing, 2018.
(116) Jamur, M. C.; Oliver, C. Cell Fixatives for Immunostaining. In *Immunocytochemical methods and protocols*; Humana Press, 2009; Vol. 588, pp. 55–61.
(117) Morris, J. K. A Formaldehyde Glutaraldehyde Fixative of High Osmolality for Use in Electron Microscopy. *J. cell Biol* **1965**, *27*, 1A-149A.
(118) Natekar, P. E.; DeSouza, F. M. Glutaraldehyde: A New Embalming Chemical Composition for Preservation of Cadavers for Innovative Surgical Procedures. *Indian J. Anat.* **2014**, *3*, 39.
(119) Bedino, J. H. Embalming Chemistry: Glutaraldehyde versus Formaldehyde. *Champion Expand. Encycl. Mortu. Pract.* **2003**, *649*, 2614–2632.
(120) Hayat, M. A. Glutaraldehyde: Role in Electron Microscopy. *Micron Microsc. Acta* **1986**, *17*, 115–135.
(121) Sabatini, D. D.; Bensch, K.; Barrnett, R. J. Cytochemistry and Electron Microscopy. The Preservation of Cellular Ultrastructure and Enzymatic Activity by Aldehyde Fixation. *J. Cell Biol.* **1963**, *17*, 19–58.
(122) Hajibagheri, M. N. *Electron Microscopy Methods and Protocols*; Humana Press, 2008.
(123) Kiernan, J. A. Formaldehyde, Formalin, Paraformaldehyde And Glutaraldehyde: What They Are And What They Do. *Micros. Today* **2000**, *8*, 8–13.
(124) Bykov, Y. S.; Cortese, M.; Briggs, J. A. G.; Bartenschlager, R. Correlative Light and Electron Microscopy Methods for the Study of Virus-Cell Interactions. *FEBS Lett.* **2016**, *590*, 1877–1895.
(125) Clancy, B.; Cauller, L. J. Reduction of Background Autofluorescence in Brain Sections Following Immersion in Sodium Borohydride. *J. Neurosci. Methods* **1998**, *83*, 97–102.
(126) Frankl, A.; Mari, M.; Reggiori, F. Electron Microscopy for Ultrastructural Analysis and Protein Localization in Saccharomyces Cerevisiae. *Microb. Cell* **2015**, *2*, 412–428.
(127) Bullen, A.; Taylor, R. R.; Kachar, B.; Moores, C.; Fleck, R. A.; Forge, A. Inner Ear Tissue Preservation by Rapid Freezing: Improving Fixation by High-Pressure Freezing and Hybrid Methods. *Hear. Res.* **2014**, *315*, 49–60.
(128) Moor, H. Snap-Freeging under High Pressure: A New Fixation Technique for Freeze-Etching. In *Proc. Fourth European Regional Conference on Electron Mocroscopy. Rome.*; 1968; Vol. 2.
(129) Moor, H. Theory and Practice of High Pressure Freezing. In *Cryotechniques in Biological Electron Microscopy*; Springer Berlin Heidelberg, 1987; pp. 175–191.

(130) Giddings, T. H.; O'Toole, E. T.; Morphew, M.; Mastronarde, D. N.; McIntosh, J. R.; Winey, M. Using Rapid Freeze and Freeze-Substitution for the Preparation of Yeast Cells for Electron Microscopy and Three-Dimensional Analysis. *Methods Cell Biol.* **2001**, *67*, 27–42.
(131) Severs, N. J. Freeze-Fracture Electron Microscopy. *Nat. Protoc.* **2007**, *2*, 547–576.
(132) Galway, M. E.; Heckman, J. W.; Hyde, G. J.; Fowke, L. C. Chapter 1: Advances in High-Pressure and Plunge-Freeze Fixation. In *Methods in Cell Biology*; Academic Press, 1995; Vol. 49, pp. 3–19.
(133) Kim, D.; Deerinck, T. J.; Sigal, Y. M.; Babcock, H. P.; Ellisman, M. H.; Zhuang, X. Correlative Stochastic Optical Reconstruction Microscopy and Electron Microscopy. *PLoS One* **2015**, *10*, e0124581.
(134) Watanabe, S.; Punge, A.; Hollopeter, G.; Willig, K. I.; Hobson, R. J.; Davis, M. W.; Hell, S. W.; Jorgensen, E. M. Protein Localization in Electron Micrographs Using Fluorescence Nanoscopy. *Nat. Methods* **2011**, *8*, 80–84.
(135) Watanabe, S.; Lehmann, M.; Hujber, E.; Fetter, R. D.; Richards, J.; Söhl-Kielczynski, B.; Felies, A.; Rosenmund, C.; Schmoranzer, J.; Jorgensen, E. M. Nanometer-Resolution Fluorescence Electron Microscopy (Nano-EM) in Cultured Cells. In *Electron Microscopy: Methods and Protocols*; Humana Press Inc., 2014; pp. 503–526.
(136) Winey, M.; Meehl, J. B.; O'Toole, E. T.; Thomas H. Giddings, J. Conventional Transmission Electron Microscopy. *Mol. Biol. Cell* **2014**, *25*, 319–323.
(137) Belazi, D.; Solé-Domènech, S.; Johansson, B.; Schalling, M.; Sjövall, P. Chemical Analysis of Osmium Tetroxide Staining in Adipose Tissue Using Imaging ToF-SIMS. *Histochem. Cell Biol.* **2009**, *132*, 105–115.
(138) Monaghan; Perusinghe; Muller. High-Pressure Freezing for Immunocytochemistry. *J. Microsc.* **1998**, *192*, 248–258.
(139) Fathali, H.; Dunevall, J.; Majdi, S.; Cans, A.-S. Extracellular Osmotic Stress Reduces the Vesicle Size While Keeping a Constant Neurotransmitter Concentration. *ACS Chem. Neurosci.* **2017**, *8*, 368–375.
(140) Tanguy, E.; Carmon, O.; Wang, Q.; Jeandel, L.; Chasserot-Golaz, S.; Montero-Hadjadje, M.; Vitale, N. Lipids Implicated in the Journey of a Secretory Granule: From Biogenesis to Fusion. *J. Neurochem.* **2016**, *137*, 904–912.
(141) Jahn, R.; Fasshauer, D. Molecular Machines Governing Exocytosis of Synaptic Vesicles. *Nature* **2012**, *490*, 201–207.
(142) Takamori, S.; Holt, M.; Stenius, K.; Lemke, E. A.; Grønborg, M.; Riedel, D.; Urlaub, H.; Schenck, S.; Brügger, B.; Ringler, P.; et al. Molecular Anatomy of a Trafficking Organelle. *Cell* **2006**, *127*, 831–

846.
(143) Südhof, T. C.; Rizo, J. Synaptic Vesicle Exocytosis. *Cold Spring Harb. Perspect. Biol.* **2011**, *3*, a005637.
(144) Jahn, R.; Scheller, R. H. SNAREs - Engines for Membrane Fusion. *Nat. Rev. Mol. Cell Biol.* **2006**, *7*, 631–643.
(145) Sutton, R.; Fasshauer, D.; Jahn, R.; Brunger, A. Crystal Structure of a SNARE Complex Involved in Synaptic Exocytosis at 2.4 Å Resolution. *Nature* **1998**, *395*, 347–353.
(146) JAHN, R.; NIEMANN, H. Molecular Mechanisms of Clostridial Neurotoxins. *Ann. N. Y. Acad. Sci.* **1994**, *733*, 245–255.
(147) Jahn, R.; Lang, T.; Südhof, T. C. Membrane Fusion. *Cell* **2003**, *112*, 519–533.
(148) Fernández-Chacón, R.; Königstorfer, A.; Gerber, S.; Garcia, J.; Matos, M.; Stevens, C.; Brose, N.; Rizo, J.; Rosenmund, C.; Sudhof, T. Synaptotagmin I Functions as a Calcium Regulator of Release Probability. *Nature* **2001**, *410*, 41–49.
(149) Koh, T. W.; Bellen, H. J. Synaptotagmin I, a Ca2+ Sensor for Neurotransmitter Release. *Trends Neurosci.* **2003**, *26*, 413–422.
(150) Vrljic, M.; Strop, P.; Ernst, J. A.; Sutton, R. B.; Chu, S.; Brunger, A. T. Molecular Mechanism of the Synaptotagmin–SNARE Interaction in Ca2+-Triggered Vesicle Fusion. *Nat. Struct. Mol. Biol.* **2010**, *17*, 325–31.
(151) Schaub, J. R.; Lu, X.; Doneske, B.; Shin, Y. K.; McNew, J. A. Hemifusion Arrest by Complexin Is Relieved by Ca2+-Synaptotagmin I. *Nat. Struct. Mol. Biol.* **2006**, *13*, 748–750.
(152) Lai, A. L.; Huang, H.; Herrick, D. Z.; Epp, N.; Cafiso, D. S. Synaptotagmin 1 and SNAREs Form a Complex That Is Structurally Heterogeneous. *J. Mol. Biol.* **2011**, *405*, 696–706.
(153) Borges, R.; Gu, C.; Machado, J. D.; Ewing, A. G. The Dynamic Nature of Exocytosis from Large Secretory Vesicles. A View from Electrochemistry and Imaging. *Cell Calcium* **2023**, *110*, 102699.
(154) Phan, N. T. N.; Li, X.; Ewing, A. G. Measuring Synaptic Vesicles Using Cellular Electrochemistry and Nanoscale Molecular Imaging. *Nat. Rev. Chem.* **2017**, *1*.
(155) Nguyen, T. D. K.; Mellander, L.; Lork, A.; Thomen, A.; Philipsen, M.; Kurczy, M. E.; Phan, N. T. N.; Ewing, A. G. Visualization of Partial Exocytotic Content Release and Chemical Transport into Nanovesicles in Cells. *ACS Nano* **2022**, *16*, 4831–4842.
(156) Larsson, A.; Majdi, S.; Oleinick, A.; Svir, I.; Dunevall, J.; Amatore, C.; Ewing, A. G. Intracellular Electrochemical Nanomeasurements Reveal That Exocytosis of Molecules at Living Neurons Is Subquantal and Complex. *Angew. Chemie* **2020**, *132*, 6777–6780.
(157) Wu, Q.; Zhang, Q.; Liu, B.; Li, Y.; Wu, X.; Kuo, S.; Zheng, L.; Wang,

C.; Zhu, F.; Zhou, Z. Dynamin 1 Restrains Vesicular Release to a Subquantal Mode In Mammalian Adrenal Chromaffin Cells. *J. Neurosci.* **2019**, *39*, 199–211.

(158) Obermüller, S.; Lindqvist, A.; Karanauskaite, J.; Galvanovskis, J.; Rorsman, P.; Barg, S. Selective Nucleotide-Release from Dense-Core Granules in Insulin-Secreting Cells. *J. Cell Sci.* **2005**, *118*, 4271–4282.

(159) Shin, W.; Arpino, G.; Thiyagarajan, S.; Su, R.; Ge, L.; McDargh, Z.; Guo, X.; Wei, L.; Shupliakov, O.; Jin, A.; et al. Vesicle Shrinking and Enlargement Play Opposing Roles in the Release of Exocytotic Contents. *Cell Rep.* **2020**, *30*, 421–431.

(160) Ren, L.; Mellander, L. J.; Keighron, J.; Cans, A.-S.; Kurczy, M. E.; Svir, I.; Oleinick, A.; Amatore, C.; Ewing, A. G. The Evidence for Open and Closed Exocytosis as the Primary Release Mechanism. *Q. Rev. Biophys.* **2016**, *49*.

(161) Wang, Y.; Ewing, A. Electrochemical Quantification of Neurotransmitters in Single Live Cell Vesicles Shows Exocytosis Is Predominantly Partial. *ChemBioChem* **2021**, *22*, 807–813.

(162) Lee, M.; Gubernator, N. G.; Sulzer, D.; Sames, D. Development of PH-Responsive Fluorescent False Neurotransmitters. *J. Am. Chem. Soc.* **2010**, *132*, 8828–8830.

(163) Lachowicz, J. E.; Sibley, D. R. Molecular Characteristics of Mammalian Dopamine Receptors. *Pharmacol. Toxicol.* **1997**, *81*, 105–113.

(164) Callier, S.; Snapyan, M.; Crom, S.; Prou, D.; Vincent, J.-D.; Vernier, P. Evolution and Cell Biology of Dopamine Receptors in Vertebrates. *Biol. Cell* **2003**, *95*, 489–502.

(165) Gnegy, M. E.; Siegel, G. J. Catecholamines. In *Basic Neurochemistry: Principles of Molecular, Cellular, and Medical Neurobiology: Eighth Edition*; Academic press, 2011; pp. 283–299.

(166) Missale, C.; Russel Nash, S.; Robinson, S. W.; Jaber, M.; Caron, M. G. Dopamine Receptors: From Structure to Function. *Physiol. Rev.* **1998**, *78*, 189–225.

(167) Fitzgerald, P.; Dinan, T. G. Prolactin and Dopamine: What Is the Connection? A Review Article. *J. Psychopharmacol.* **2008**, *22*, 12–19.

(168) Dominguez, N.; Estevez-Herrera, J.; Borges, R.; Machado, J. D. The Interaction between Chromogranin A and Catecholamines Governs Exocytosis. *FASEB J.* **2014**, *28*, 4657–4667.

(169) He, X.; Ewing, A. G. Simultaneous Counting of Molecules in the Halo and Dense-Core of Nanovesicles by Regulating Dynamics of Vesicle Opening. *Angew. Chemie* **2022**, *134*, e202116217.

(170) Ren, L.; Oleinick, A.; Svir, I.; Amatore, C.; Ewing, A. G. Amperometric Measurements and Dynamic Models Reveal a Mechanism for How Zinc Alters Neurotransmitter Release. *Angew.*

Chemie Int. Ed. **2020**, *59*, 3083–3087.

(171) Omiatek, D. M.; Dong, Y.; Heien, M. L.; Ewing, A. G. Only a Fraction of Quantal Content Is Released during Exocytosis as Revealed by Electrochemical Cytometry of Secretory Vesicles. *ACS Chem. Neurosci.* **2010**, *1*, 234–245.

(172) Lovrić, J.; Dunevall, J.; Larsson, A.; Ren, L.; Andersson, S.; Meibom, A.; Malmberg, P.; Kurczy, M. E.; Ewing, A. G. Nano Secondary Ion Mass Spectrometry Imaging of Dopamine Distribution Across Nanometer Vesicles. *ACS Nano* **2017**, *11*, 3446–3455.

(173) van den Dries, K.; Fransen, J.; Cambi, A. Fluorescence CLEM in Biology: Historic Developments and Current Super-resolution Applications. *FEBS Lett.* **2022**, *596*, 2486–2496.

(174) Bucana, C.; Hoyer, L. C.; Hobbs, B.; Breesman, S.; McDaniel, M.; Hanna Jr, M. G. Morphological Evidence for the Translocation of Lysosomal Organelles from Cytotoxic Macrophages into the Cytoplasm of Tumor Target Cells1 | Cancer Research | American Association for Cancer Research. *Cancer Res.* **1976**, *36*, 4444–4458.

(175) Santarella-Mellwig, R.; Haselmann, U.; Schieber, N. L.; Walther, P.; Schwab, Y.; Antony, C.; Bartenschlager, R.; Romero-Brey, I. Correlative Light Electron Microscopy (CLEM) for Tracking and Imaging Viral Protein Associated Structures in Cryo-Immobilized Cells. *J. Vis. Exp.* **2018**, *139*, 58154.

(176) Amato, P. A.; Unanue, E. R.; Taylor, D. L. Distribution of Actin in Spreading Macrophages: A Comparative Study on Living and Fixed Cells. *J. Cell Biol.* **1983**, *96*, 750–761.

(177) Wouters, C. H.; Koerten, H. K.; Bonnet, J.; Daems, W. T.; Ploem, J. S. Quantitative DNA Measurements in an Instrument Combining Scanning Electron Microscopy and Light Microscopy. *J. Microsc.* **1986**, *141*, 41–53.

(178) Kukulski, W.; Schorb, M.; Kaksonen, M.; Briggs, J. A. G. Plasma Membrane Reshaping during Endocytosis Is Revealed by Time-Resolved Electron Tomography. *Cell* **2012**, *150*, 508–520.

(179) Polishchuk, R. S.; Polishchuk, E. V.; Marra, P.; Alberti, S.; Buccione, R.; Luini, A.; Mironov, A. A. Correlative Light-Electron Microscopy Reveals the Tubular-Saccular Ultrastructure of Carriers Operating between Golgi Apparatus and Plasma Membrane. *J. Cell Biol.* **2000**, *148*, 45–58.

(180) Jun, S.; Ke, D.; Debiec, K.; Zhao, G.; Meng, X.; Ambrose, Z.; Gibson, G. A.; Watkins, S. C.; Zhang, P. Direct Visualization of HIV-1 with Correlative Live-Cell Microscopy and Cryo-Electron Tomography. *Structure* **2011**, *19*, 1573–1581.

(181) Luby-Phelps, K.; Ning, G.; Fogerty, J.; Besharse, J. C. Visualization of Identified GFP-Expressing Cells by Light and Electron Microscopy.

J. Histochem. Cytochem. **2003**, *51*, 271–274.
(182) Begemann, I.; Galic, M. Correlative Light Electron Microscopy: Connecting Synaptic Structure and Function. *Front. Synaptic Neurosci.* **2016**, *8*, 28.
(183) Betzig, E.; Patterson, G. H.; Sougrat, R.; Lindwasser, O. W.; Olenych, S.; Bonifacino, J. S.; Davidson, M. W.; Lippincott-Schwartz, J.; Hess, H. F. Imaging Intracellular Fluorescent Proteins at Nanometer Resolution. *Science.* **2006**, *313*, 1642–1645.
(184) Musat, N.; Foster, R.; Vagner, T.; Adam, B.; Kuypers, M. M. M. Detecting Metabolic Activities in Single Cells, with Emphasis on NanoSIMS. *FEMS Microbiol. Rev.* **2012**, *36*, 486–511.
(185) Musat, N.; Musat, F.; Weber, P. K.; Pett-Ridge, J. Tracking Microbial Interactions with NanoSIMS. *Curr. Opin. Biotechnol.* **2016**, *41*, 114–121.
(186) Truckenbrodt, S.; Viplav, A.; Jähne, S.; Vogts, A.; Denker, A.; Wildhagen, H.; Fornasiero, E. F.; Rizzoli, S. O. Newly Produced Synaptic Vesicle Proteins Are Preferentially Used in Synaptic Transmission. *EMBO J.* **2018**, *37*, e98044.
(187) Jähne, S.; Mikulasch, F.; Heuer, H. G. H.; Truckenbrodt, S.; Agüi-Gonzalez, P.; Grewe, K.; Vogts, A.; Rizzoli, S. O.; Priesemann, V. Presynaptic Activity and Protein Turnover Are Correlated at the Single-Synapse Level. *Cell Rep.* **2021**, *34*, 108841.
(188) Li, T.; Wu, T.-D.; Mazéas, L.; Toffin, L.; Guerquin-Kern, J.-L.; Leblon, G.; Bouchez, T. Simultaneous Analysis of Microbial Identity and Function Using NanoSIMS. *Environ. Microbiol.* **2008**, *10*, 580–588.
(189) Kültz, D. Defining Biological Stress and Stress Responses Based on Principles of Physics. *J. Exp. Zool. Part A Ecol. Integr. Physiol.* **2020**, *333*, 350–358.
(190) Kültz, D. Evolution of Cellular Stress Response Mechanisms. *Journal of Experimental Zoology Part A: Ecological and Integrative Physiology*, 2020, *333*, 359–378.
(191) Abramowicz, A.; Widłak, P.; Pietrowska, M. Different Types of Cellular Stress Affect the Proteome Composition of Small Extracellular Vesicles: A Mini Review. *Proteomes* **2019**, *7*, 23.
(192) Ritossa, F. A New Puffing Pattern Induced by Temperature Shock and DNP in Drosophila. *Experientia* **1962**, *18*, 571–573.
(193) Craig, E. A.; Schlesinger, M. J. The Heat Shock Respons. *Crit. Rev. Biochem.* **1985**, *18*, 239–280.
(194) Fulda, S.; Gorman, A. M.; Hori, O.; Samali, A. Cellular Stress Responses: Cell Survival and Cell Death. *Int. J. Cell Biol.* **2010**.
(195) Hetz, C.; Zhang, K.; Kaufman, R. J. Mechanisms, Regulation and Functions of the Unfolded Protein Response. *Nature Reviews*

Molecular Cell Biology, 2020, *21*, 421–438.
(196) Kaufman, R. J. Orchestrating the Unfolded Protein Response in Health and Disease. *J. Clin. Invest.* **2002**, *110*, 1389–1398.
(197) Schröder, M.; Kaufman, R. J. The Mammalian Unfolded Protein Response. *Annu. Rev. Biochem.* **2005**, *74*, 739–789.
(198) Marciniak, S. J.; Chambers, J. E.; Ron, D. Pharmacological Targeting of Endoplasmic Reticulum Stress in Disease. *Nat. Rev. Drug Discov.* **2022**, *21*, 115–140.
(199) Wolozin, B.; Ivanov, P. Stress Granules and Neurodegeneration. *Nat. Rev. Neurosci.* **2019**, *20*, 649–666.
(200) Tolay, N.; Buchberger, A. Role of the Ubiquitin System in Stress Granule Metabolism. *International Journal of Molecular Sciences*, 2022, *23*, 3624.
(201) Anderson, P.; Kedersha, N. Stress Granules: The Tao of RNA Triage. *Trends in Biochemical Sciences*, 2008, *33*, 141–150.
(202) Kedersha, N.; Cho, M. R.; Li, W.; Yacono, P. W.; Chen, S.; Gilks, N.; Golan, D. E.; Anderson, P. Dynamic Shuttling of TIA-1 Accompanies the Recruitment of MRNA to Mammalian Stress Granules. *J. Cell Biol.* **2000**, *151*, 1257–1268.
(203) Zhang, Y.; Gu, J.; Sun, Q. Aberrant Stress Granule Dynamics and Aggrephagy in Als Pathogenesis. *Cells*, 2021, *10*, 2247.
(204) Wood, A.; Gurfinkel, Y.; Polain, N.; Lamont, W.; Lyn Rea, S. Molecular Mechanisms Underlying TDP-43 Pathology in Cellular and Animal Models of ALS and FTLD. *International journal of molecular sciences*, 2021, *22*, 4705.
(205) Buchan, J. R.; Kolaitis, R. M.; Taylor, J. P.; Parker, R. Eukaryotic Stress Granules Are Cleared by Autophagy and Cdc48/VCP Function. *Cell* **2013**, *153*, 1461.
(206) Tauber, D.; Tauber, G.; Parker, R. Mechanisms and Regulation of RNA Condensation in RNP Granule Formation. *Trends in Biochemical Sciences*, 2020, *45*, 764–778.
(207) Reineke, L. C.; Dougherty, J. D.; Pierre, P.; Lloyd, R. E. Large G3BP-Induced Granules Trigger EIF2α Phosphorylation. *Mol. Biol. Cell* **2012**, *23*, 3499–3510.
(208) Kedersha, N.; Panas, M. D.; Achorn, C. A.; Lyons, S.; Tisdale, S.; Hickman, T.; Thomas, M.; Lieberman, J.; McInerney, G. M.; Ivanov, P.; et al. G3BP–Caprin1–USP10 Complexes Mediate Stress Granule Condensation and Associate with 40S Subunits. *J. Cell Biol.* **2016**, *212*.
(209) Protter, D. S. W.; Parker, R. Principles and Properties of Stress Granules. *Trends Cell Biol.* **2016**, *26*, 668–679.
(210) Jain, S.; Wheeler, J. R.; Walters, R. W.; Agrawal, A.; Barsic, A.; Parker, R. ATPase-Modulated Stress Granules Contain a Diverse

Proteome and Substructure. *Cell* **2016**, *164*, 487–498.
(211) Bley, N.; Lederer, M.; Pfalz, B.; Reinke, C.; Fuchs, T.; Glaß, M.; Möller, B.; Hüttelmaier, S. Stress Granules Are Dispensable for MRNA Stabilization during Cellular Stress. *Nucleic Acids Res.* **2015**, *43*, 26.
(212) Yang, P.; Mathieu, C.; Kolaitis, R. M.; Zhang, P.; Messing, J.; Yurtsever, U.; Yang, Z.; Wu, J.; Li, Y.; Pan, Q.; et al. G3BP1 Is a Tunable Switch That Triggers Phase Separation to Assemble Stress Granules. *Cell* **2020**, *181*, 325–345.
(213) Namkoong, S.; Ho, A.; Woo, Y. M.; Kwak, H.; Lee, J. H. Systematic Characterization of Stress-Induced RNA Granulation. *Mol. Cell* **2018**, *70*, 175-187.e8.
(214) Lin, Y.; Protter, D. S. W.; Rosen, M. K.; Parker, R. Formation and Maturation of Phase-Separated Liquid Droplets by RNA-Binding Proteins. *Mol. Cell* **2015**, *60*, 208–219.
(215) Ross, C. A.; Poirier, M. A. Protein Aggregation and Neurodegenerative Disease. *Nat. Med.* **2004**, *10 Suppl*, S10-7.
(216) Aguzzi, A.; O'Connor, T. Protein Aggregation Diseases: Pathogenicity and Therapeutic Perspectives. *Nat. Rev. Drug Discov.* **2010**, *9*, 237–248.
(217) Forman, M. S.; Trojanowski, J. Q.; Lee, V. M. Y. Neurodegenerative Diseases: A Decade of Discoveries Paves the Way for Therapeutic Breakthroughs. *Nat. Med.* **2004**, *10*, 1055–1063.
(218) Xu, S.; Gierisch, M. E.; Schellhaus, A. K.; Poser, I.; Alberti, S.; Salomons, F. A.; Dantuma, N. P. Cytosolic Stress Granules Relieve the Ubiquitin-proteasome System in the Nuclear Compartment. *EMBO J.* **2022**, *42*, e111802.
(219) Dudman, J.; Qi, X. Stress Granule Dysregulation in Amyotrophic Lateral Sclerosis. *Front. Cell. Neurosci.* **2020**, *14*, 598517.
(220) Cleveland, D.; Rothstein, J. From Charcot to Lou Gehrig: Deciphering Selective Motor Neuron Death in Als. *Nat. Rev. Neurosci.* **2001**, *2*, 806–819.
(221) Brown, R. H.; Al-Chalabi, A. Amyotrophic Lateral Sclerosis. *N. Engl. J. Med.* **2017**, *377*, 162–172.
(222) Nedelsky, N. B.; Taylor, J. P. Bridging Biophysics and Neurology: Aberrant Phase Transitions in Neurodegenerative Disease. *Nat. Rev. Neurol.* **2019**, *15*, 272–286.
(223) Neumann, M.; Sampathu, D. M.; Kwong, L. K.; Truax, A. C.; Micsenyi, M. C.; Chou, T. T.; Bruce, J.; Schuck, T.; Grossman, M.; Clark, C. M.; et al. Ubiquitinated TDP-43 in Frontotemporal Lobar Degeneration and Amyotrophic Lateral Sclerosis. *Science.* **2006**, *314*, 130–133.
(224) Vance, C.; Rogelj, B.; Hortobágyi, T.; De Vos, K. J.; Nishimura, A.

L.; Sreedharan, J.; Hu, X.; Smith, B.; Ruddy, D.; Wright, P.; et al. Mutations in FUS, an RNA Processing Protein, Cause Familial Amyotrophic Lateral Sclerosis Type 6. *Science.* **2009**, *323*, 1208–1211.

(225) Liu-Yesucevitz, L.; Bilgutay, A.; Zhang, Y. J.; Vanderwyde, T.; Citro, A.; Mehta, T.; Zaarur, N.; McKee, A.; Bowser, R.; Sherman, M.; et al. Tar DNA Binding Protein-43 (TDP-43) Associates with Stress Granules: Analysis of Cultured Cells and Pathological Brain Tissue. *PLoS One* **2010**, *5*, e13250.

(226) McDonald, K. K.; Aulas, A.; Destroismaisons, L.; Pickles, S.; Beleac, E.; Camu, W.; Rouleau, G. A.; Velde, C. Vande. TAR DNA-Binding Protein 43 (TDP-43) Regulates Stress Granule Dynamics via Differential Regulation of G3BP and TIA-1. *Hum. Mol. Genet.* **2011**, *20*, 1400–1410.

(227) Cao, J.; Zhong, M. B.; Toro, C. A.; Zhang, L.; Cai, D. Endo-Lysosomal Pathway and Ubiquitin-Proteasome System Dysfunction in Alzheimer's Disease Pathogenesis. *Neurosci. Lett.* **2019**, *703*, 68–78.

(228) González, A. E.; Muñoz, V. C.; Cavieres, V. A.; Bustamante, H. A.; Cornejo, V. H.; Januário, Y. C.; González, I.; Hetz, C.; Dasilva, L. L.; Rojas-Fernández, A.; et al. Autophagosomes Cooperate in the Degradation of Intracellular C-Terminal Fragments of the Amyloid Precursor Protein via the MVB/Lysosomal Pathway. *FASEB J.* **2017**, *31*, 2446–2459.

(229) Xu, W.; Fang, F.; Ding, J.; Wu, C. Dysregulation of Rab5-Mediated Endocytic Pathways in Alzheimer's Disease. *Traffic* **2018**, *19*, 253–262.

(230) Xue, S.; Jia, J. Genetic Association between Ubiquitin Carboxy-Terminal Hydrolase-L1 Gene S18Y Polymorphism and Sporadic Alzheimer's Disease in a Chinese Han Population. *Brain Res.* **2006**, *1087*, 28–32.

(231) Zhang, Y.; Chen, X.; Zhao, Y.; Ponnusamy, M.; Liu, Y. The Role of Ubiquitin Proteasomal System and Autophagy-Lysosome Pathway in Alzheimer's Disease. *Rev. Neurosci.* **2017**, *28*, 861–868.

(232) Cherkasov, V.; Grousl, T.; Theer, P.; Vainshtein, Y.; Gläßer, C.; Mongis, C.; Kramer, G.; Stoecklin, G.; Knop, M.; Mogk, A.; et al. Systemic Control of Protein Synthesis through Sequestration of Translation and Ribosome Biogenesis Factors during Severe Heat Stress. *FEBS Lett.* **2015**, *589*, 3654–3664.

(233) Kedersha, N. L.; Gupta, M.; Li, W.; Miller, I.; Anderson, P. RNA-Binding Proteins TIA-1 and TIAR Link the Phosphorylation of EIF-2α to the Assembly of Mammalian Stress Granules. *J. Cell Biol.* **1999**, *147*, 1431–1441.

(234) Van Treeck, B.; Parker, R. Principles of Stress Granules Revealed by

Imaging Approaches. *Cold Spring Harb. Perspect. Biol.* **2019**, *11*.
(235) Souquere, S.; Mollet, S.; Kress, M.; Dautry, F.; Pierron, G.; Weil, D. Unravelling the Ultrastructure of Stress Granules and Associated P-Bodies in Human Cells. *J. Cell Sci.* **2009**, *122*, 3619–3626.